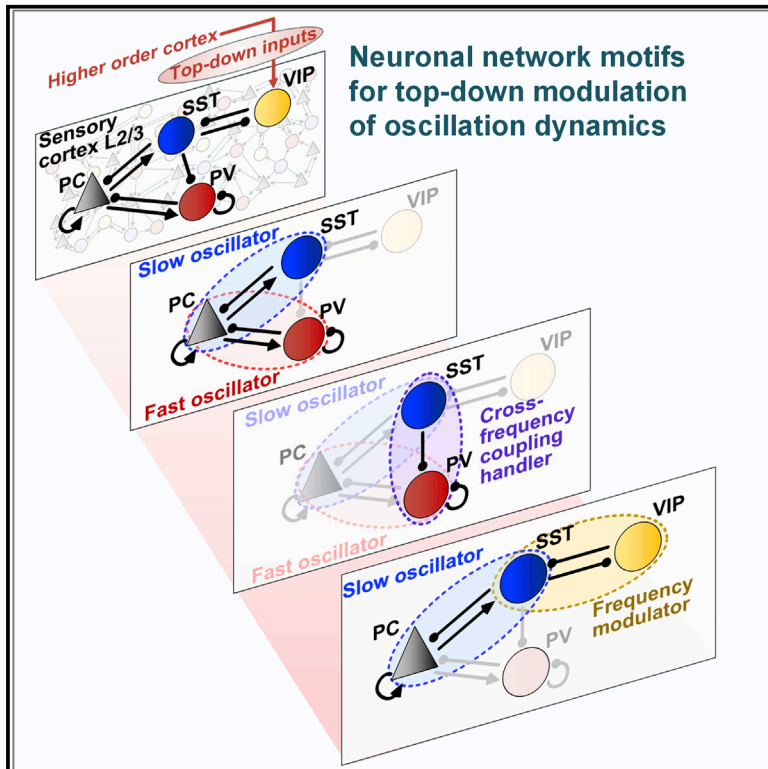


Combined Positive and Negative Feedback Allows Modulation of Neuronal Oscillation Frequency during Sensory Processing

Graphical Abstract



Authors

Byeongwook Lee, Dongkwan Shin,
Steven P. Gross, Kwang-Hyun Cho

Correspondence

ckh@kaist.ac.kr

In Brief

Lee et al. discover that precisely organized synaptic connectivity among cortical pyramidal cells and various classes of interneurons (expressing SST, VIP, and PV) enables sensitive frequency modulation of slow oscillations to encode top-down inputs and results in cross-frequency coupling with bottom-up-mediated fast oscillations.

Highlights

- A computational neuronal circuit model of sensory cortex layers 2 and 3 is constructed
- Cooperation of SST, VIP, and PV cells determines neuronal oscillation dynamics
- The core structure regulating the top-down modulation of slow oscillation is found
- The feedback between SST and VIP cells determines adaptability to top-down input



Combined Positive and Negative Feedback Allows Modulation of Neuronal Oscillation Frequency during Sensory Processing

Byeongwook Lee,¹ Dongkwan Shin,¹ Steven P. Gross,² and Kwang-Hyun Cho^{1,3,*}

¹Laboratory for Systems Biology and Bio-inspired Engineering, Department of Bio and Brain Engineering, Korea Advanced Institute of Science and Technology (KAIST), Daejeon 34141, Republic of Korea

²Department of Developmental and Cell Biology, UC Irvine, Irvine, CA 92697, USA

³Lead Contact

*Correspondence: ckh@kaist.ac.kr

<https://doi.org/10.1016/j.celrep.2018.10.029>

SUMMARY

A key step in sensory information processing involves modulation and integration of neuronal oscillations in disparate frequency bands, a poorly understood process. Here, we investigate how top-down input causes frequency changes in slow oscillations during sensory processing and, in turn, how the slow oscillations are combined with fast oscillations (which encode sensory input). Using experimental connectivity patterns and strengths of interneurons, we develop a system-level model of a neuronal circuit controlling these oscillatory behaviors, allowing us to understand the mechanisms responsible for the observed oscillatory behaviors. Our analysis discovers a circuit capable of producing the observed oscillatory behaviors and finds that a detailed balance in the strength of synaptic connections is the critical determinant to produce such oscillatory behaviors. We not only uncover how disparate frequency bands are modulated and combined but also give insights into the causes of abnormal neuronal activities present in brain disorders.

INTRODUCTION

Cognitive processes—including attention, memory formation, and sensory processing—are tightly correlated with neuronal oscillations involving multiple timescales. Depending on top-down influences, oscillations in the low-frequency range (3–20 Hz) undergo context-dependent frequency modulations, which deliver specific commands of the higher-order cortex, suggesting that sensitive frequency modulation plays a crucial role in cognitive processes by rendering neuronal communication effective, precise, and selective (Bastos et al., 2015; Engel et al., 2001; Fries, 2015; Kilavik et al., 2012; Michalareas et al., 2016). Indeed, these frequency changes likely coordinate specific cortical functions, such as stimulus selection (Schroeder and Lakatos, 2009), multi-sensory integration (van Atteveldt et al., 2014), and motor planning (Rickert et al., 2005) through combining with fast neuronal oscillations (>20 Hz; phenomenon referred to as “cross-fre-

quency coupling” [CFC]), which typically encode sensory stimuli (Canolty and Knight, 2010; Hyafil et al., 2015; Schroeder and Lakatos, 2009). CFC has recently received attention due to its participation in cognitive processing (Hyafil et al., 2015). Not surprisingly, altered oscillatory behaviors (e.g., abnormal frequency modulation of slow oscillations and abnormal CFC) are reported to cause cognitive deficits in various brain disorders (Basar-Eroglu et al., 2008; Hong et al., 2004; Javitt, 2009; Koh et al., 2011; Marco et al., 2011). However, in spite of such experimental interest and demonstrated importance, how slow oscillations are modulated, and how their combination with fast oscillations is controlled, remains unclear.

Although exactly how these oscillatory behaviors are formed and controlled remains unclear, we do know *spatially* where these processes occur: in the superficial layers (layers 2 and 3) of the sensory cortex (Chen et al., 2017). Layers 2 and 3 of the sensory cortex play a central role in sensory processing as they receive and integrate local feedforward inputs (i.e., bottom-up sensory inputs) and top-down inputs from other cortical areas (Harris and Mrsic-Flogel, 2013; Karnani et al., 2016; Lee et al., 2013; Zhang et al., 2014). In particular, the cortico-cortical top-down inputs to layers 2 and 3 are thought to be crucial for context-dependent sensory processing (Bastos et al., 2015; Harris and Mrsic-Flogel, 2013; Lee et al., 2013; Zhang et al., 2014).

Sensory processing is likely to be reflected in the spiking activity of neurons, and synchronized oscillatory firing activity of pyramidal cells (PCs) at various frequencies has been typically detected in layers 2 and 3 of the sensory cortex (Chen et al., 2017; Womelsdorf et al., 2014). Although multiple features contribute to determining the firing activity of PCs, the contribution of the three largest inhibitory interneurons (INs), which represent 90% of INs in layers 2 and 3 of the sensory cortex, has gained much attention (Pfeffer et al., 2013). Somatostatin-expressing INs (SST INs) and parvalbumin-expressing INs (PV INs) have been shown to contact PCs and mediate synchronized oscillatory activity of PCs in distinct frequency ranges (with SST INs mediating oscillations in the 5- to 30-Hz range and PV INs mediating oscillations in the >20-Hz range; Chen et al., 2017). Moreover, vasoactive intestinal-peptide-expressing INs (VIP INs) are the main recipients of top-down input from higher-order cortex and mediate disinhibition of PCs through inhibiting SST INs (Lee et al., 2013; Pi et al., 2013; Zhang et al., 2014).



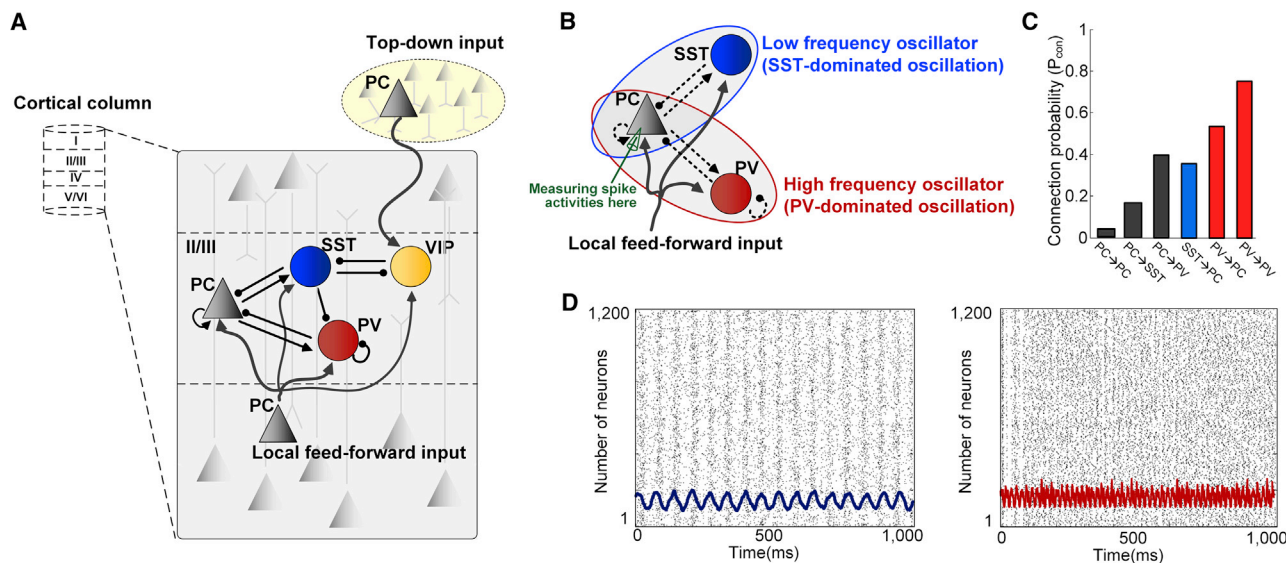


Figure 1. Neuronal Circuit Comprised of Heterogeneous Interneuron Classes in Layers 2 and 3 of the Sensory Cortex

(A) Schematic of the neuronal circuit created by the three interneuron (IN) classes and excitatory pyramidal cells (PCs). Inputs to modulate the circuit’s activity come from the higher order cortex (top-down input) and the inter-layer (local feedforward input).

(B) Schematic of the nested oscillators (NF_{PC-SST} in blue and NF_{PC-PV} in red). PCs participate in the generation of both SST-dominated oscillation (in theta to beta range) and PV-dominated oscillation (in gamma range).

(C) Connection probabilities (P_{con}) of pathways within NF_{PC-SST} and NF_{PC-PV} were chosen to mediate two distinct synchronized oscillatory activities of the PCs.

(D) Spike rasters show the spike times of the PC population in each oscillator, reflecting the ensemble dynamics. With the assigned P_{con} over the pathways, NF_{PC-SST} generates an 18-Hz oscillation (left, blue) and NF_{PC-PV} generates a 75-Hz oscillation (right, red).

These three IN classes (i.e., SST, VIP, and PV INs) were recently shown to form specific synaptic connections with distinct connection strengths (Figure S1) that define a specifically organized synaptic circuit (Pfeffer et al., 2013; Figure 1A). However, an understanding of the functional ramification of the specific connectivity properties for each IN class is still lacking (Schröter et al., 2017). Here, we investigated exactly this, that is, how specific connectivity properties of these three IN classes contribute to modulate slow oscillations and further control CFC between slow and fast oscillations.

Overall, we identified two particularly important substructures—(1) interlinked positive and negative feedback structure among VIP INs, SST INs, and PCs and (2) unidirectional synaptic inhibition of SST INs acting on PV INs—which, together with the connection strengths that hold them together, are optimally designed to generate, modulate, and combine the crucial oscillatory behaviors required for sensory processing. Thus, our analysis discovered how the circuit in layers 2 and 3 intrinsically generates oscillations; second, how it maximizes the frequency modulation sensitivity of slow oscillations to top-down input; and finally, how it allows stable CFC between slow and fast oscillations.

RESULTS

Construction of a Computational Interneuron Circuit Model Found in Layers 2 and 3 of the Sensory Cortex

We constructed a computational spiking neural circuit that reflects the experimentally measured connectivity properties of

the comprising neuronal classes (Figure 1A; Pfeffer et al., 2013). Each neuronal class was modeled by taking experimentally determined electrophysiological membrane properties and the population distribution in layers 2 and 3 of the sensory cortex (see Method Details). Two excitatory Poisson inputs representing a local feedforward (bottom-up) and long-range top-down input were given to the circuit (see Method Details). To exclusively examine the effect of top-down influence (which is represented by top-down input strength) on the circuit dynamic, the local feedforward input was kept constant in time and the top-down input strength was varied (see Method Details). By examining various combinations of connection probability (P_{con}) between pre- and postsynaptic neuronal populations, we directly linked each combination to the response properties of PCs for varying top-down input strength. Especially, we focused on generating a “rhythmic mode” operation (Bastos et al., 2015; Chen et al., 2017; Michalareas et al., 2016; Womelsdorf et al., 2014; i.e., functions in an oscillatory-based regime), which occurs in layers 2 and 3 of the sensory cortex. We thus searched for a combination of P_{con} among the pathways that (1) generates slow and fast oscillations, (2) modulates frequency of slow oscillation over varying top-down input strength, and finally (3) creates CFC between slow and fast oscillations. Finally, we compared theoretical behavior of our model with these chosen values to experimentally determined data.

First, we noticed that the circuit contains two nested negative feedback (NF) structures, NF_{PC-SST} and NF_{PC-PV} (Figure 1B), where PCs are involved in both NF structures. NF structures involving PCs and INs are ubiquitously found in neuronal

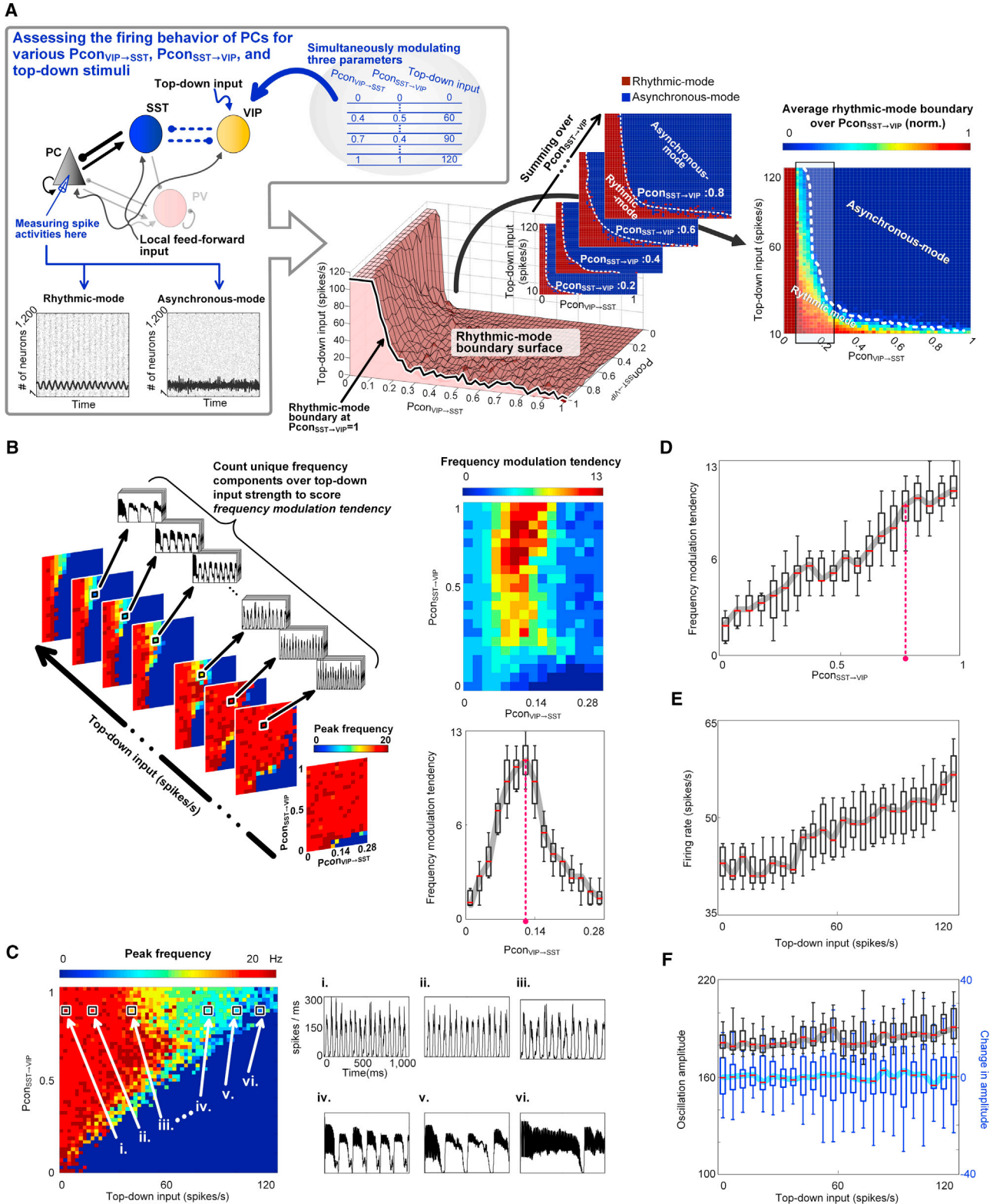


Figure 2. Frequency Modulation Mediated by an Interlinked Positive and Negative Feedback Structure among Pyramidal Cells, SST Interneurons, and VIP Interneurons

(A) Schematic with a sub-circuit of the circuit in Figure 1A, indicating an interlinked positive and negative feedback (IPNF) structure. After determining the $P_{con_{PC \rightarrow SST}}$ and $P_{con_{SST \rightarrow PC}}$ for $NF_{PC \rightarrow SST}$ to act as an oscillator (Figure 1C), we now include positive feedback (PF) by including the interactions with the VIP INs, (legend continued on next page)

networks. Because they have been proposed to generate oscillatory activity (Prill et al., 2005; Wilson and Cowan, 1972), we hypothesized that here these structures might participate in generating the observed collective slow (3–20 Hz) and fast (>20 Hz) oscillations in layers 2 and 3 of the sensory cortex (Chen et al., 2017). Moreover, additional work found that the peak frequency of the NF structure is primarily determined by the specific balance of connectivity strengths for pathways within the structure (Börgers and Kopell, 2003; Brunel and Wang, 2003; Shin and Cho, 2013). As noted above, modulating P_{con} allows control of synaptic connectivity strengths, thus, in principle, allowing us to tune the oscillation frequencies for the two NF structures, NF_{PC-SST} and NF_{PC-PV} . We denote the connectivity strengths for these substructures as $P_{con_{NF}}$. We chose a particular $P_{con_{NF}}$ for each pathway (Figure 1C) that generates highly synchronized oscillatory activities of the PCs (see Figure S2 and Method Details for details). With such $P_{con_{NF}}$, in response to local feed-forward input, the NF_{PC-SST} generated an 18-Hz oscillation (Figure 1D, left) and the NF_{PC-PV} generated a 75-Hz oscillation (Figure 1D, right), within the frequency ranges of typical beta and gamma oscillations, respectively, and consistent with experimentally determined frequencies (Chen et al., 2017). As such, we kept $P_{con_{NF}}$ fixed for all further analyses.

The Synaptic Structure Constructed by Distinct Connectivity Patterns of VIP Interneurons, SST Interneurons, and PCs Meets the Structural Prerequisite for High Adaptability to Top-Down Input

Because PV INs are considered to contribute more on encoding bottom-up sensory input rather than top-down input, we initially excluded the PV INs from the circuit to investigate the circuit's top-down processing. Thus, we focused on the part of the circuit that includes VIP INs, SST INs, and PCs. Intriguingly, we observed that these three neuronal classes are connected by positive-plus-negative feedback structures (Figure 2A, left). Although a single negative feedback structure can produce sustained oscillations, and single negative and positive feedback structures are found in some biological networks (Eshaghi et al., 2010; Gouzé, 1998; Kim et al., 2007, 2010; Kim and Cho, 2006; Murray et al., 2010; Park et al., 2006; Shin et al., 2006; Sreenath

et al., 2008; Tsai et al., 2008), many biological oscillators employ coupled feedback structures, as observed in eukaryotic cell cycle (Pomeroy et al., 2005), circadian clocks (Lee et al., 2000), and the p53-Mdm2 oscillator (Harris and Levine, 2005). Generally speaking, the presence of positive feedback combined with negative feedback increases adaptability to various stimuli and creates greater frequency tunability over a wider stimulus range than a simple negative feedback structure, while maintaining a constant oscillation amplitude (Tian et al., 2009; Tsai et al., 2008). Layers 2 and 3 of the sensory cortex also requires this functional characteristic (i.e., a high degree of adaptability to stimuli), as they are the major targets of top-down input from higher-order cortex and have a central role in sensory processing. Thus, high-frequency tunability by top-down input would be preferable for the sensory cortex, to increase communication diversity and allow selective communication with other brain regions for top-down-influenced (i.e., context-dependent) sensory processing. Notably, the interlinked positive and negative feedback (IPNF) structure among VIP INs, SST INs, and PCs satisfy the structural prerequisite for high adaptability to top-down input.

The Interlinked Positive and Negative Feedback Structure of VIP-SST-PC Enables Frequency Modulation with a Constant Amplitude

We were intrigued by the presence of the IPNF structure in layers 2 and 3 of the sensory cortex because this structure has never been reported in neuronal networks. Integrating positive feedback, $PF_{SST-VIP}$, with the negative feedback structure, NF_{PC-SST} , that we found likely to generate the beta oscillation might then allow frequency tuning of this oscillation in response to top-down stimuli. Because diverse responses can arise from the same structure depending on its context, here we wanted to assess the adaptability of the IPNF structure to varying top-down stimuli: is it able to respond to a broad range of such stimuli and, if so, which aspects of the network contribute to this ability. We hypothesized that, to have high adaptability, the IPNF structure should first maintain (but modulate) the intrinsic oscillatory behavior of NF_{PC-SST} over wide top-down input strengths. To investigate, we first explored the importance of the feedback

$PF_{SST-VIP}$. We examined under what conditions the population activity of the PCs exhibits oscillatory behavior (i.e., rhythmic mode) versus asynchronous behavior (i.e., asynchronous mode) by varying $P_{con_{VIP \rightarrow SST}}$, $P_{con_{SST \rightarrow VIP}}$, and top-down input strength (left). We obtained the rhythmic mode boundary surface, which is defined as an upper limit of parameter combinations ($P_{con_{VIP \rightarrow SST}}$, $P_{con_{SST \rightarrow VIP}}$, and top-down input strength) that generated the rhythmic mode (middle). Rhythmic mode boundaries between top-down input strength and $P_{con_{VIP \rightarrow SST}}$ at different $P_{con_{SST \rightarrow VIP}}$ are compared (middle up). The color of each voxel indicates whether the particular parameter combination is designated as rhythmic mode (red) or asynchronous mode (blue). By summing the status of each voxel (either rhythmic mode or asynchronous mode) and averaging over all $P_{con_{SST \rightarrow VIP}}$ values, the average rhythmic mode boundary over $P_{con_{SST \rightarrow VIP}}$ was obtained (right). The color code represents the relative abundance of the number of times each voxel had rhythmic mode status over $P_{con_{SST \rightarrow VIP}}$. Shaded box indicates the range of $P_{con_{VIP \rightarrow SST}}$ that the rhythmic mode maintains over the wide top-down stimuli (right).

(B) An example illustration of calculating the frequency modulation tendency (FMT) of the IPNF structure (left). The FMT of the IPNF structure with particular $P_{con_{VIP \rightarrow SST}}$ and $P_{con_{SST \rightarrow VIP}}$ was examined (right up). Within the $P_{con_{SST \rightarrow VIP}}$ range of 0.6–0.9, the FMT exhibited a bell-shaped change over $P_{con_{VIP \rightarrow SST}}$ (right bottom). The pink line indicates the optimal $P_{con_{VIP \rightarrow SST}}$ that maximizes the FMT of the IPNF structure.

(C) Modulation of the oscillation frequency over increasing $P_{con_{SST \rightarrow VIP}}$ and top-down input strengths, with a fixed $P_{con_{VIP \rightarrow SST}}$ of 0.12, is plotted (left). The oscillation frequency modulates in a stepwise manner over the top-down input increment. Example evolution of the spike-time histogram of PCs under different top-down input strengths is plotted (right).

(D) The FMT of the IPNF structure increased linearly with increasing $P_{con_{SST \rightarrow VIP}}$. The pink line indicates the optimal $P_{con_{SST \rightarrow VIP}}$ that maximizes the FMT.

(E) Firing rates of PCs increase as the strength of top-down input increases.

(F) IPNF structure provides a constant oscillation amplitude and the oscillation frequency varies along with top-down input strengths. Data are represented as box-and-whisker plots.

strength of the positive feedback (PF), $PF_{SST \rightarrow VIP}$ module, by changing connectivity strengths of the $PF_{SST \rightarrow VIP}$ (i.e., $P_{con_{VIP \rightarrow SST}}$ and $P_{con_{SST \rightarrow VIP}}$) and strengths of top-down input and then assessing the impact of such changes by using numerical simulations to determine whether the population of PCs exhibits rhythmic mode under each condition (Figure 2A, left). If the PCs do exhibit such a rhythmic mode, we further examined the frequency values (see Method Details). One goal of exploring the effect of changes in these parameter values was to understand a surprising experimental observation: there is a distinct disparity of the measured connectivity strengths in $PF_{SST \rightarrow VIP}$ (weak $VIP \rightarrow SST$ connectivity strength and strong $SST \rightarrow VIP$ strength; Pfeffer et al., 2013).

By examining the whole parameter space, we were able to determine the range of PF parameters over which the NF-derived rhythmic mode persists; its boundary was defined as an upper limit of the $P_{con_{VIP \rightarrow SST}}$ and $P_{con_{SST \rightarrow VIP}}$ combinations that maintained the rhythmic mode in response to top-down stimuli (Figure 2A, middle). Intriguingly, we found that the rhythmic mode of $NF_{PC \rightarrow SST}$ is maintained over a relatively wide top-down input strength only for a low $P_{con_{VIP \rightarrow SST}}$ (i.e., for $P_{con_{VIP \rightarrow SST}} < 0.3$; Figure 2A, right).

As we identified that the $VIP \rightarrow SST$ pathway with the specific range of $P_{con_{VIP \rightarrow SST}}$ contributes on maintaining rhythmic mode for wide top-down input, we now investigated the contribution of the $SST \rightarrow VIP$ pathway in deciding the adaptability of the IPNF structure. As mentioned above, in general, it is likely that, for context-dependent sensory processing, a functional control circuit should display sensitive frequency modulation of PCs to varying top-down stimuli (i.e., high adaptability). To quantitatively explore this, and in particular the contribution of the strength of the $SST \rightarrow VIP$ pathway to the frequency modulation, we analyzed the actual frequency values that were obtained at the boundary surface (Figure 2A, right). We developed a metric we call the “frequency modulation tendency,” or FMT, to measure the adaptability of the IPNF structure. The FMT of the IPNF structure was calculated by counting the number of different frequency values that appear over different top-down input strengths at particular $P_{con_{SST \rightarrow VIP}}$ (Figures 2B, left, and S3; see Method Details). Thus, a high FMT can be interpreted as a high “top-down stimuli-to-unique frequency” mapping ability. We investigated how the FMT varies as the $P_{con_{SST \rightarrow VIP}}$ changes and searched for optimal $P_{con_{SST \rightarrow VIP}}$ that resulted in maximum FMT. While modulating $P_{con_{SST \rightarrow VIP}}$, we confined the analysis space to $P_{con_{VIP \rightarrow SST}} < 0.3$ to maintain the rhythmic mode (see above). We found that the FMT of the IPNF structure is determined by the balance between $P_{con_{VIP \rightarrow SST}}$ and $P_{con_{SST \rightarrow VIP}}$ (Figure 2B, right top). Our results (Figures 2B–2D) imply that the relatively weak connectivity strength of the $VIP \rightarrow SST$ pathway and the relatively strong connectivity strength of the $SST \rightarrow VIP$ pathway, in terms of connection probability, are the conditions for maximizing the frequency modulation capability of the IPNF structure. We plotted some of the example evolution of the spike-time histogram of PCs at $P_{con_{VIP \rightarrow SST}} = 0.12$ and $P_{con_{VIP \rightarrow SST}} = 0.8$ (Figure 2C). Oscillation frequency modulated from the peak frequency of $NF_{PC \rightarrow SST}$ to lower frequency in a stepwise manner under increasing top-down input strength (Figure 2C).

Ultimately, we picked $P_{con_{VIP \rightarrow SST}} = 0.12$ and $P_{con_{SST \rightarrow VIP}} = 0.8$ as the optimal P_{con} to accomplish high FMT of the IPNF structure (plotted with a pink line in Figures 2B, right bottom, and 2D).

Under the tuned P_{con} s over the pathways for the maximum frequency tunability, other characteristics of the neuronal population activities exposed by the IPNF structure were examined. As top-down input to VIP INs was increased, the mean firing rates of PCs increased as previously reported (Lee et al., 2013; Figure 2E). Furthermore, the IPNF structure enabled the adjustment of the oscillation frequency while maintaining the amplitude of the oscillation approximately constant, which is an intriguing characteristic caused by the VIP INs recruiting top-down inputs (Figure 2F). Such a characteristic plays a crucial role in allowing slow oscillations to form reliable and well-controlled CFC with fast oscillations; this is discussed in more detail later.

The Lack of Self-Inhibition in SST and VIP Interneurons Enables Flexible Frequency Modulation

One notable difference between the SST INs, VIP INs, and PV INs is their self-inhibition preference: there are strong self-inhibitory connections among PV INs, but the opposite is true for the SST INs and VIP INs (Lee et al., 2013; Pfeffer et al., 2013). In the context of the previously studied negative feedback loop involving PV INs and PCs ($NF_{PC \rightarrow PV}$), which is ubiquitously found in all brain regions and known to typically encode sensory input, several studies reported on the phenomenological attributes of strong self-inhibition on PV INs (Bartos et al., 2007; Buzsáki and Wang, 2012; Deleuze et al., 2014): inclusion of self-inhibition connections among PV INs in $NF_{PC \rightarrow PV}$ provides more precise control over the activity of the PV INs, resulting in generation of highly synchronized gamma oscillations. Because such oscillations become more vulnerable to noise as the frequency increases, high firing synchrony of PV INs would be desirable for gamma oscillations to ensure their reliability of information transmission within and between brain regions. However, no study has yet suggested functional consequences—and advantages, if any—due to SST INs and VIP INs avoiding self-inhibition connections.

To determine the ramifications of the weak self-inhibition preferences of SST INs and VIP INs, we used our FMT metric (see above): we increased $P_{con_{SST \rightarrow SST}}$ and $P_{con_{VIP \rightarrow VIP}}$, respectively (Figures 3A and 3C) and determined how that changed the IPNF structure’s response to various top-down input strengths (see Method Details). Overall, we found that increasing self-inhibition resulted in significant impairment of FMT (Figures 3B, 3D, and S4). As an example, as we increased $P_{con_{SST \rightarrow SST}}$, the FMT of the IPNF structure declined dramatically (Figure 3B). In sum, the IPNF circuit’s activity is differentially sensitive to inclusion of self-inhibition connections to the SST INs and VIP INs (i.e., there are different minimum strengths of self-inhibition required to observe significant effects); however, their effects are qualitatively similar: they both result in a reduced FMT of the IPNF structure. These results thus provide an explanation for the experimentally observed lack of self-inhibitory connections: self-inhibition is lacking to maximize the FMT of the IPNF structure. Therefore, in the model, we set the optimal

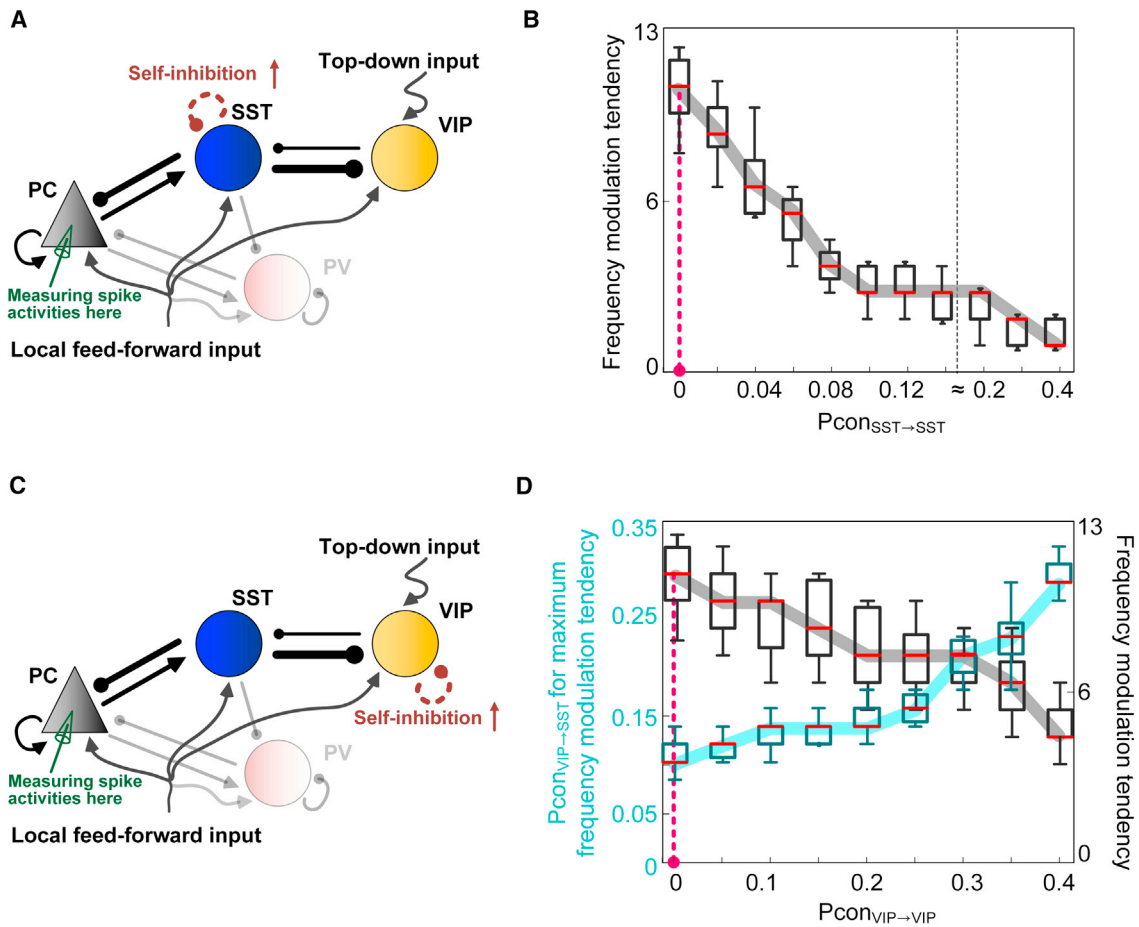


Figure 3. Effect of Increasing Self-Inhibition Strength in SST and VIP Interneurons on Determining the Frequency Modulation Tendency of the IPNF Structure

(A) Schematic of the IPNF structure, highlighting possible self-inhibition of SST interneurons (INs). The strength of the self-inhibition was determined by the value of $P_{con_{SST \rightarrow SST}}$.

(B) As $P_{con_{SST \rightarrow SST}}$ increases, the population activity of the PCs increasingly remains at the inherent characteristic peak frequency generated by the NF_{PC-SST} , which leads to a decrease in the FMT of the IPNF structure. Optimal $P_{con_{SST \rightarrow SST}}$ value that provides the maximum FMT is plotted with pink line.

(C) Schematic of the IPNF structure, highlighting possible self-inhibition of VIP INs. The strength of the self-inhibition was controlled by varying $P_{con_{VIP \rightarrow VIP}}$.

(D) As the $P_{con_{VIP \rightarrow VIP}}$ increases, a larger $P_{con_{VIP \rightarrow SST}}$ is required (turquoise) to maximize FMT of the IPNF structure. However, increasing $P_{con_{VIP \rightarrow SST}}$ eventually reduces the FMT of the IPNF structure (black), which was shown in our previous result (Figure 2B, right bottom). Optimal $P_{con_{VIP \rightarrow VIP}}$ value that provides the maximum FMT is plotted with pink line. Data are represented as box-and-whisker plots.

P_{con} of the $SST \rightarrow SST$ and $VIP \rightarrow VIP$ pathway to zero, as they provide the maximum frequency modulation capability to the IPNF structure.

Incorporation of Bottom-Up Influences by PV INs

So far, we identified the IPNF structure as the core structure for top-down-mediated frequency modulation of the slow oscillations observed in layers 2 and 3. However, another factor may affect the FMT of the IPNF structure: the PV INs actually form a negative feedback loop with PCs and thus deliver bottom-up influences to the PCs (Figure 4A, left). So, unlike the above simplified model where the activity of PCs was solely influenced by SST INs, here (and in actuality) the PCs receive influences from PV INs as well, and thus the FMT of the IPNF structure is likely affected by inclusion of the PV INs.

Mechanistically, previous experiments found that gamma oscillations of the PV INs are controlled by the top-down-mediated slow oscillations (Bastos et al., 2015; Fries, 2015), suggesting that the FMT of the IPNF should remain high with inclusion of PV INs. To unravel the specific conditions under which PV INs meaningfully contribute to the overall circuit function for sensory processing, we thus analyzed an extended model, which included PV INs in the IPNF structure (Figure 4A, left). Specifically, we first examined how inclusion of the PV INs affects the FMT of the IPNF structure. Increases in the top-down input to the VIP INs reduce the activity of the SST INs, which in turn release the PV INs from inhibition by the SST INs. This decrement in SST INs activity allows the PV INs to start influencing the activity of PCs and indeed become the dominant population that governs the PCs' activity. We named

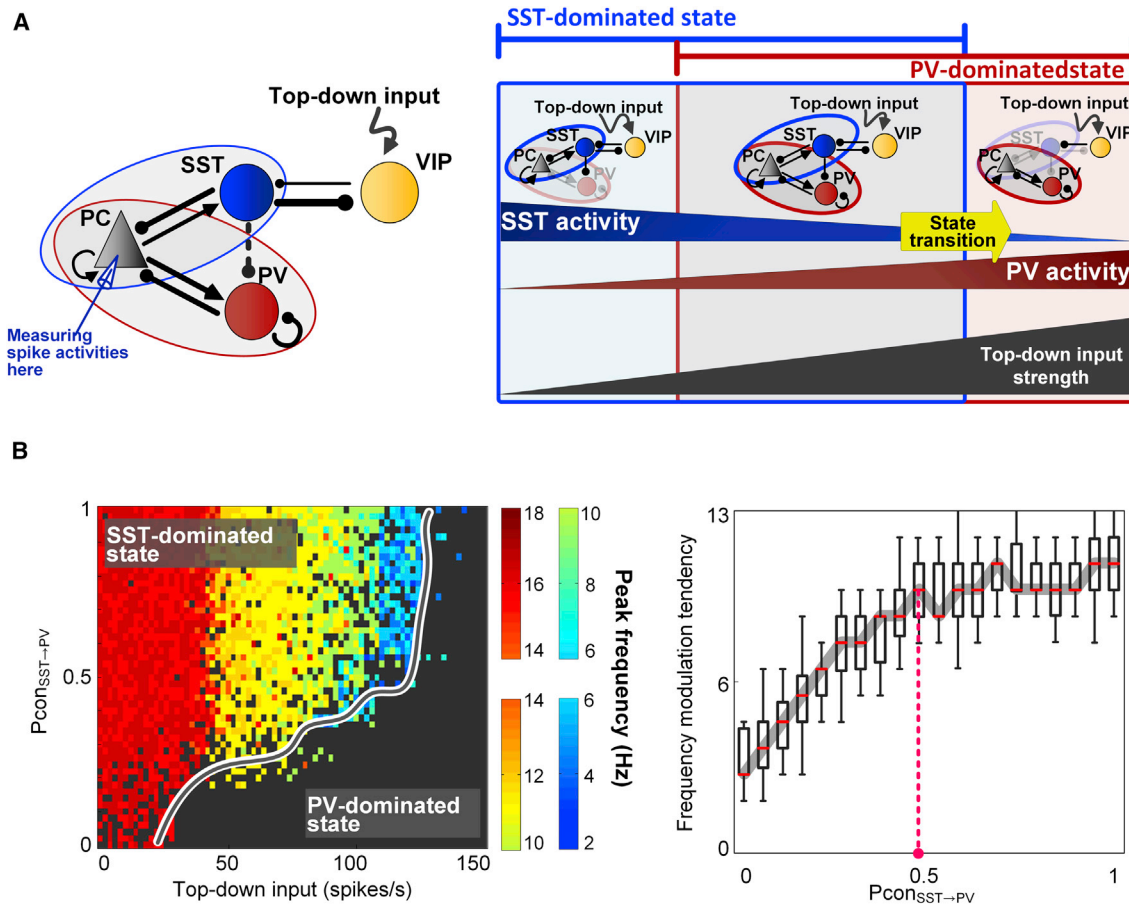


Figure 4. Variation in the Frequency Modulation Tendency of the IPNF Structure by Inclusion of SST → PV Pathway

(A) Schematic of the whole circuit (left). Increases in the top-down input to the VIP INs reduces the activity of the SST INs, which in turn releases the PV INs from inhibition by the SST INs. This decrease in the activity of the SST INs eventually causes the PV INs to become the dominant population that governs the PCs' activity and mediates state transition (right).

(B) Variation in the FMT of the IPNF structure when it is in the SST-dominated state, as a function of the strength of the SST → PV linkage, controlled by increasing $P_{con_{SST \rightarrow PV}}$. The transition to the PV-dominated state with high-frequency oscillations occurs as a function both of $P_{con_{SST \rightarrow PV}}$ and of the strength of top-down input (left). The FMT of the IPNF structure only increases with $P_{con_{SST \rightarrow PV}}$ up to a critical $P_{con_{SST \rightarrow PV}}$ value of 0.5 (right). The pink line indicates the optimal $P_{con_{SST \rightarrow PV}}$ that maximizes the FMT. Data are represented as box-and-whisker plots.

this phenomenon a “state transition” from “SST-dominated state” to “PV-dominated state” (Figure 4A, right). This gradual shift of PCs' activity dominance eventually affects the FMT of the IPNF structure. Because the SST → PV pathway most directly controls the activity of PV INs, we examined changes in the FMT of the IPNF structure due to modulation of $P_{con_{SST \rightarrow PV}}$. Intriguingly, we found that excess value of $P_{con_{SST \rightarrow PV}}$ is not functional. That is, although increasing $P_{con_{SST \rightarrow PV}}$ to 0.5 increases the overall frequency tunability, when $P_{con_{SST \rightarrow PV}}$ exceeds this value, it no longer affects the frequency tunability of the IPNF structure (Figure 4B, left), because increased inhibition from the VIP INs to the SST INs caused the activities of the SST INs to decrease to a level that NF_{PC-SST} could no longer sustain the SST-dominated oscillations. We thus chose $P_{con_{SST \rightarrow PV}} = 0.5$ as the optimal P_{con} to carry out the frequency modulation process (plotted with a pink line in Figure 4B, right). In summary, we built a model

that determines the adaptability of the circuit with taking both top-down and bottom-up influences into account.

Top-Down-Mediated Slow Oscillations Control Bottom-Up-Mediated Fast Oscillations via Precisely Tuned Synaptic Connectivity

Now that we have created a model whose architecture is derived from experiments, with connectivity strengths, in terms of connection probability, optimized to have high adaptability to top-down inputs (Figure 5A), we wanted to use the extended model to better understand experimentally observed CFC, i.e., the ability of slow oscillations to affect fast ones. We examined spike rasters that reflect population-level activity of the four neuronal populations under five specific top-down input strengths. The PCs, SST INs, and VIP INs exhibited a global oscillatory behavior where the strength of top-down input determines the unique oscillation frequency of the PCs' firing activity

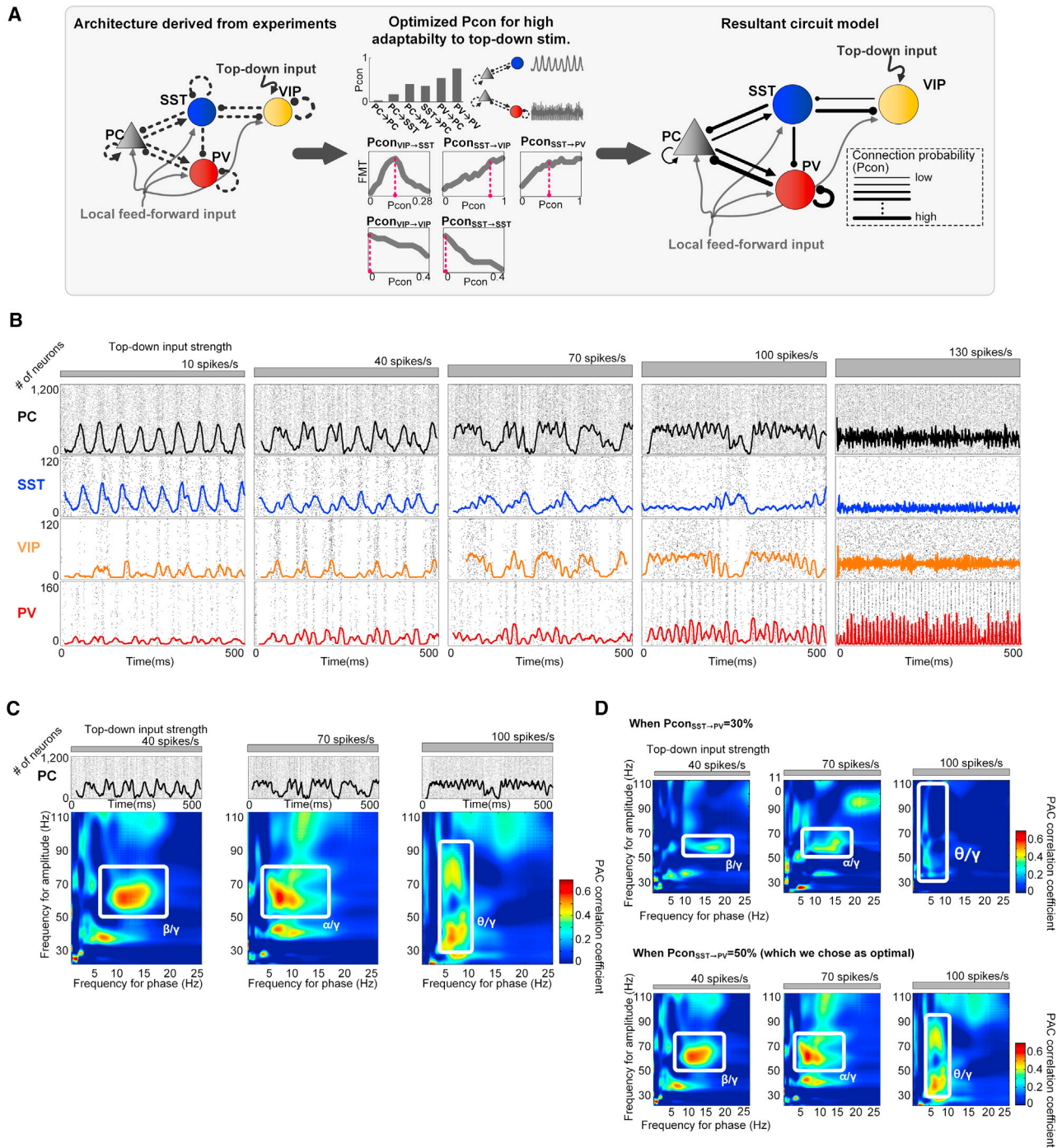


Figure 5. The Activity Profiles of Four Neuronal Classes

(A) Diagram of the circuit, with the optimal connectivity strength (in terms of Pcon) of each pathway, obtained by the simulation analysis, to maximize the FMT of the IPNF structure (i.e., high adaptability to top-down input).

(B) Spike rasters, reflecting ensemble activity of the four neuronal populations, as a function of different top-down input strengths. During the SST-dominated state, PCs, SST INs, and VIP INs show synchronized population activity, where their oscillation frequencies decrease along with the increase of top-down input. When top-down input increases to the level where SST INs can no longer control PV INs, PV INs become a dominant IN population that controls the firing pattern of PCs.

(C) The strength of phase-amplitude coupling (PAC) is quantified for the PCs' oscillatory activities that arise at a top-down input strength of 40 spikes/s, 70 spikes/s, and 100 spikes/s.

(D) Quantification of the change of the PAC strength along with the strength of the SST→PV pathway.

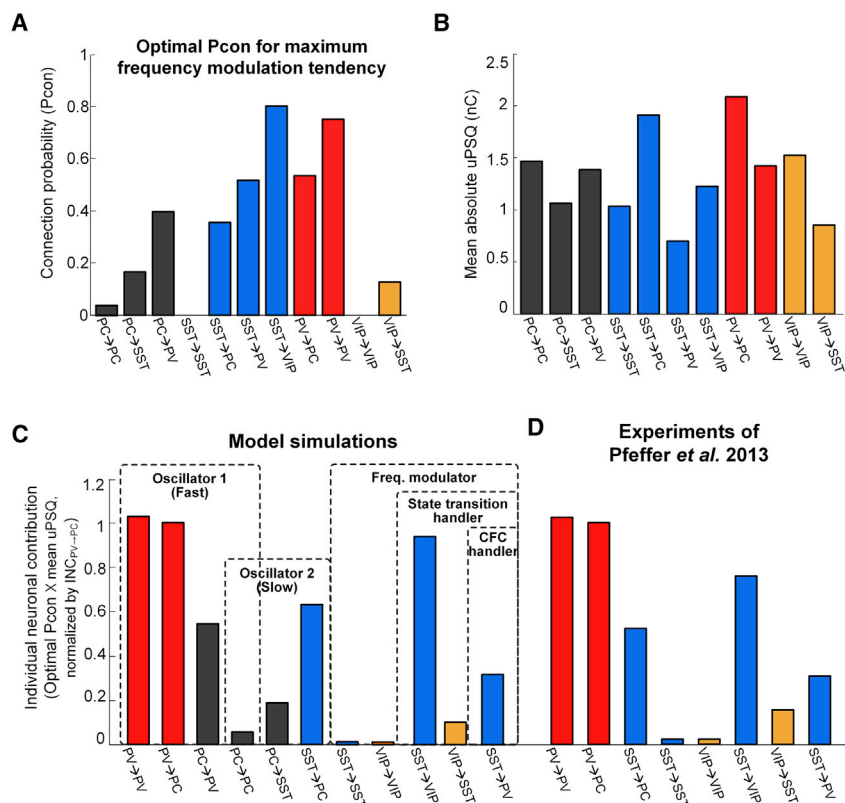


Figure 6. Connectivity Strengths based on Theoretical Model Simulations and Experimental Recordings

(A) The optimal Pcon values for each pathway in the circuit, obtained by the simulation analysis, under the hypothesis that, for optimal performance, the circuit should provide maximum frequency modulation tendency.

(B) Estimated mean unitary postsynaptic charge (uPSQ) (the time integral of unitary postsynaptic current) of the synaptic connections among the four different neuronal classes.

(C) Theoretical INC values obtained by multiplying Pcon of (A) and mean uPSQ of (B).

(D) Experimentally measured INC values in the visual cortex layers 2 and 3 (values adapted from Figure 7A in Pfeffer et al. 2013). It can be seen that the INC values over the pathways are similar between theoretically obtained values and experimental values. This result is thus consistent with the hypothesis that, *in vivo*, synaptic connectivity strengths in the pathways within the circuit have evolved to the optimal values that not only provide high adaptability to the top-down input but also provide stable CFC between sensory information (i.e., top-down command and bottom-up sensory stimuli).

(Figure 5B). Most importantly, the firing pattern of PV INs—and its subsequent influence on the PCs—was controlled by the activity of SST INs mediated by top-down input through the SST → PV pathway. As a result, the CFC appeared as the top-down input strength to VIP INs was increased (40 spikes/s to 70 spikes/s and 100 spikes/s). We explored this CFC in more detail by quantifying the strength of phase-amplitude coupling (PAC) (see Method Details), which experimentally is the most widely observed type of CFC between slow and fast oscillations (Hyafil et al., 2015). We quantified the PAC strength of PCs' oscillatory activities in Figure 5B (via top-down input strength of 40 spikes/s, 70 spikes/s, and 100 spikes/s). As the top-down input strength increased, we observed a phase shift of strong PAC from β/γ to α/γ to θ/γ (Figure 5C). Finally, because our analysis highlighted the critical role of SST activity in controlling PV activity, we explored this more by altering the $P_{con_{SST \rightarrow PV}}$ and investigating its effect on PAC (Figure 5D). Indeed, the SST-PV coupling strength played a critical role in facilitating the PAC: the weak $P_{con_{SST \rightarrow PV}}$ produced weak PCA (Figure 5D, top) whereas the $P_{con_{SST \rightarrow PV}}$ of 0.5, which we chose as the optimal value to maintain high FMT of the IPNF, also ensured strong PAC (Figure 5D, bottom). In summary, although a number of synaptic architectures were previously suggested for generation of PAC (Hyafil et al., 2015), none considered the role of SST → PV pathway, which we find plays a dominant role.

Regulation of oscillation amplitude during frequency modulation is another important feature for brain function. In particular, co-modulation of amplitude and frequency has been widely

observed during frequency modulation in fast oscillations (i.e., gamma range; Jadi and Sejnowski, 2014). However, interestingly, our analysis suggests that the IPNF structure keeps the slow oscillation amplitude approximately constant during frequency modulation, which is an intriguing characteristic caused by the VIP INs recruiting top-down input (Figure 2F). To explore the functional importance of this unique feature, especially in respect to PAC efficiency, we considered a simplified oscillator model (Figure S5; see Method Details). Interestingly, there was superior PAC efficiency when the slow oscillation amplitude was kept constant during frequency modulation (Figure S6). Benefits of this property are discussed below (see Discussion). Taken all together, our analysis provides a circuit-level explanation of the previous experimental observations in terms of a cooperative mechanism arising from interactions between diverse IN classes.

Link to Previous Experiments

By studying the circuit's dynamic response to top-down input, we discovered that a specific balance of synaptic connectivity strengths (in terms of Pcons; Figure 6A) could yield the rhythmic mode operation for encoding a wide range of top-down input by modulating the frequency of the SST-dominated oscillation in theta to beta range. Because these Pcons were derived by simulation analysis of the model circuit, under the appealing but untested hypothesis that the system was optimized for frequency modulation sensitivity of slow oscillations to top-down input, we wanted to test whether this was actually consistent with experimentally measured synaptic connectivity strengths. Pfeffer et al. (2013) determined the synaptic connectivity

strengths between SST INs, VIP INs, and PV INs in the visual cortex layers 2 and 3. They used a measurement called the individual neuronal contribution (INC), which is the product of the Pcon between the pre- and postsynaptic neuronal classes and the average unitary postsynaptic charge (uPSQ) (the time integral of the unitary postsynaptic current) generated by a single presynaptic spike. We estimated the average uPSQ between the pre- and postsynaptic neuronal classes by using previous electrophysiological recordings (Avermann et al., 2012; Figure 6B; see Method Details). By multiplying the Pcon (Figure 6A) and estimated uPSQ (Figure 6B), we represented the synaptic connectivity strength of each pathway obtained by the simulation analysis in terms of the INC value (Figure 6C). We found that the estimated INC values of our model are consistent with the experimental INC values of Pfeffer et al. (2013; Figure 6D), suggesting that our hypothesis that the connectivity properties of the circuit might have organized to perform high-frequency tunability to encode top-down inputs (i.e., high adaptability) is reasonable. In particular, a distinct disparity of the connectivity strengths over the SST→VIP and VIP→SST pathways support the maximum FMT of the IPNF structure for the SST-dominated slow oscillation. Moreover, we found that the experimentally determined $INC_{SST \rightarrow PV}$ is consistent with our model value, suggesting that top-down and bottom-up influences are properly integrated to perform sensory processing. Moreover, the unique synaptic connectivity strength of $INC_{SST \rightarrow PV}$ suggests that the brain circuit has evolved to consider the wiring economy for its computational needs and make pertinent (i.e., neither too weak nor unnecessarily strong) synaptic connections. Importantly, taken together, our results suggest that the importance of synaptic connections cannot be determined solely by their strengths, because a certain synaptic connectivity strength has meaning primarily not in isolation but rather as it affects the network's function.

DISCUSSION

The superficial layers (layers 2 and 3) of the sensory cortex play a central role in sensory processing by receiving and integrating bottom-up and top-down inputs from other layers (within the sensory cortex) and other cortical areas (Harris and Mrsic-Flogel, 2013; Jones and Wise, 1977; Lee et al., 2013; Zhang et al., 2014). In particular, top-down inputs from the higher-order cortex are considered crucial for context-dependent sensory processing (Bastos et al., 2015; Diamond et al., 2008; Harris and Mrsic-Flogel, 2013; Lee et al., 2013; Zhang et al., 2014). Interestingly, synchronized oscillatory firing activities of PCs at various frequencies within the theta to beta range are typically detected in layers 2 and 3 (Bastos et al., 2015; Chen et al., 2017; Michalar-eas et al., 2016; Womelsdorf et al., 2014), suggesting that distinct oscillation frequencies encode the context-dependent sensory processing. Furthermore, modulations of bottom-up-mediated gamma oscillation by these top-down-mediated slow oscillations are also detected in this area (Bastos et al., 2015; Fries, 2015), suggesting an integration capability of the area. Considering the crucial role of layers 2 and 3 in sensory processing, a circuit-level systematic understanding of these phenomena is of paramount importance. Nonetheless, although

the neuronal classes composing this area—and their interconnection properties—have been reported, because they form a complex feedback structure, it had previously not been possible to use this experimental information to understand the ensemble's function.

Throughout this paper, we attempted to explain the physiological regime (i.e., the origin of the observed frequencies and how those frequencies are modulated and combined) in layers 2 and 3 of the sensory cortex. By analyzing the patterns of synaptic connectivity in relation to the response properties of PCs, we found that connectivity patterns with specific connectivity strengths are designed to support a maximum frequency tunability according to the top-down input strength, enabling top-down demands to be encoded in distinct frequency components. The IPNF structure we identify, formed by VIP INs, SST INs, and PCs, is a key frequency modulator for the top-down input, where VIP INs preferentially recruit top-down inputs.

From this analysis, various intriguing experimentally observed connectivity properties could now be rationalized. For instance, we find that the weak connectivity strength of the VIP→SST pathway is required to sustain synchronized oscillatory activity for PCs (Figure 2A, right). Moreover, the strong connectivity strength of the SST→VIP pathway is required to broaden the frequency modulation range to encode top-down inputs (Figure 2D). Our model helps understand the reason for the curious absence of self-inhibition in SST INs and VIP INs: it contributes to achievement of sensitive frequency modulation (Figures 3B and 3D). Moreover, the intermediate connectivity strength of the SST→PV pathway is an optimal value that both maximizes the frequency modulation capability of the IPNF structure among VIP-SST-PCs (Figure 4B) and also ensures stable cross-frequency coupling between top-down-mediated slow oscillations and bottom-up-mediated fast oscillations (Figure 5D). As seen in our extensive simulation results, alteration of even a single pathway can strongly influence the outcome of the circuit (i.e., frequency tunability and integration of slow and fast oscillations), indicating that interactions among neuronal classes should be very specifically tuned for a particular function.

Notably, our study thus adds perspective on how frequency modulation of the slow oscillation occurs. Previously, the frequency modulation of the slow oscillation was mainly considered as a consequence of electrical coupling among the SST INs (Fanselow et al., 2008; Urban-Ciecko and Barth, 2016), which is an intrinsic property, that is, independent of the external stimulus. However, such mechanism was suggested before the synaptic interaction properties of SST INs with neighboring neuronal classes were revealed. Considering the recent experimental findings that SST INs are connected with VIP INs, which are the main recipients of the top-down input, experiments might thus lead one to suppose that the role of synaptic interactions of SST INs with neighboring neuronal classes must now be re-considered as one attempts to understand top-down influences on the SST-dominated oscillations. Thus, we developed such an integrated approach and identified a synaptic mechanism of the frequency modulation process.

The best-known mechanism of long-range input recruitment to local regional circuits is via PCs, but recent experimental results show long-range projection to various IN classes

(Womelsdorf and Everling, 2015). Determining the precise functional consequences brought about by different IN classes recruiting long-range cortico-cortical inputs has been a major challenge in neuroscience research (Womelsdorf and Everling, 2015). In the case of layers 2 and 3 of the sensory cortex, in contrast to the other two IN classes, VIP INs are the main recipients of top-down input. As an exclusive functional consequence of the VIP INs recruiting long-range inputs, we revealed that the oscillation frequency of the SST-dominated theta to beta range could be adjusted without compromising the oscillation amplitude, which is an extraordinary characteristic. In contrast, as mentioned above, PV INs recruit preferential input from the thalamus to pyramidal-interneuron gamma structure (PING) and thereby modulate oscillation frequency within the gamma range (Jadi and Sejnowski, 2014). During this frequency modulation process, substantial changes in the oscillation amplitude occur as well (Jadi and Sejnowski, 2014). Because co-modulation of amplitude and frequency occurs in the gamma range, why is frequency modulation with a constant amplitude required in the low (i.e., theta to beta) frequency range? We believe it serves to avoid cross-talk. That is, different low-frequency band oscillations are caused by distinct top-down demands and ultimately often control the gamma range oscillation through CFC to carry out diverse cognitive functions (Canolty and Knight, 2010; Schroeder and Lakatos, 2009). For reliable and effective CFC, the low-frequency band oscillations should keep constant amplitudes over a range of frequencies such that diverse top-down information is robustly processed against various disturbances (Figures S5 and S6). Taken together, the IPNF structure and its long-range input recruitment from the higher order cortex to the VIP INs enables the low-frequency band oscillations in theta to beta range to reliably control the gamma oscillations and to further process various cognitive functions by allowing flexible frequency modulation over a constant amplitude.

By providing a quantitative model of this critical brain processes, our model creates a platform to better understand disease processes. In particular, our rhythmic mode boundary surface analysis (Figure 2A, middle) provides a rough disease-relevant map of parameter values: any choice of parameters, from electrophysiological properties of individual neurons to the connection probabilities between different neuronal classes, that move the system across the boundary and destroy the rhythmic mode should result in disease. In principle, using measured cellular-level changes occurring in specific disease processes, one can then use the model to determine how the system's function is altered, and thus, one can start to link specific functional changes to physiologically observed symptoms, leading to a clearer view of the disease and also potentially suggesting new therapeutic approaches (Assmus et al., 2006).

Although it provides an important framework for further studies, we note that our model is incomplete: frequency modulation within gamma range in layers 2 and 3 of the sensory cortex by PV INs was not considered. Although such frequency modulation of gamma range oscillation is also important, as it reflects bottom-up sensory stimulus, it is beyond the scope of this study, which instead was investigating top-down-mediated frequency modulation of slow oscillations. However, a previous modeling study suggested that the frequency of the gamma range oscillation

can be regulated by the relative strength of two distinct excitatory pathways to the PV INs (i.e., monosynaptic and disynaptic pathways; Jadi and Sejnowski, 2014). Based on recent experimental results showing that PV INs preferentially receive additional strong excitatory inputs from the thalamus (Cruikshank et al., 2007; Yang et al., 2013), we assume that these strong inputs may mediate the frequency modulation within the gamma range.

Another limitation is that our study is based on numerical investigation. Although the model is well defined and robust, the approach is inherently insufficient to provide a detailed mechanistic-level explanation for the models' dynamic properties. For such insight, future analytic investigation is required, where analytical solutions directly connect the mechanisms and parameters to dynamic properties.

Various feedback structures are ubiquitously observed in different types of biological networks, including gene regulatory networks, molecular networks, and neuronal networks, and are the building blocks that perform distinct functions. A few intriguing cases in which different biological networks share similar feedback structures have been identified, and these feedback structures perform similar functions (Alon, 2006; Milo et al., 2002). This functional similarity raises the possibility that evolution may have converged on similar circuits in different biological networks to perform important signal processing functions (Alon, 2006; Milo et al., 2002). The functional role of the IPNF structure in the brain network has not been reported, making our work the exemplar of a neuronal structure able to modulate oscillation frequency according to top-down demands while maintaining constant amplitude. Although we focused on layers 2 and 3 of the sensory cortex, recent studies suggest that other cortical regions share strikingly commonalities in constituent cell types and their intrinsic properties (Harris and Mrsic-Flogel, 2013; Schröter et al., 2017). Therefore, the IPNF structure may turn out to be a general frequency modulator structure in multiple brain areas.

STAR★METHODS

Detailed methods are provided in the online version of this paper and include the following:

- KEY RESOURCES TABLE
- CONTACT FOR REAGENT AND RESOURCE SHARING
- METHOD DETAILS
 - Network model
 - Synaptic interaction modeling
 - External inputs
 - Conditions for generating oscillations in NF_{PC-SST} and NF_{PC-PV}
 - Characterization of oscillations
 - Frequency modulation tendency
 - Quantification of phase-amplitude coupling
 - Quantification of noise vulnerability of phase-amplitude coupling with respect to amplitude-frequency relationships of slow oscillations
 - Data analysis
- QUANTIFICATION AND STATISTICAL ANALYSIS
- DATA AND SOFTWARE AVAILABILITY

SUPPLEMENTAL INFORMATION

Supplemental Information includes six figures and two tables and can be found with this article online at <https://doi.org/10.1016/j.celrep.2018.10.029>.

ACKNOWLEDGMENTS

This work was supported by the National Research Foundation of Korea (NRF) grants funded by the Korea Government, the Ministry of Science and ICT (2017R1A2A1A17069642 and 2015M3A9A7067220), and also supported by the Samsung Research Funding Center of Samsung Electronics (SRFC-IT1401-05).

AUTHOR CONTRIBUTIONS

K.-H.C. designed the project and supervised the research; B.L., D.S., and K.-H.C. performed the modeling and analysis; and B.L., D.S., S.P.G., and K.-H.C. wrote the manuscript.

DECLARATION OF INTERESTS

The authors declare no competing interests.

Received: January 5, 2018

Revised: May 21, 2018

Accepted: October 3, 2018

Published: November 6, 2018

REFERENCES

- Alon, U. (2006). *An Introduction to Systems Biology: Design Principles of Biological Circuits* (CRC).
- Assmus, H.E., Herwig, R., Cho, K.-H., and Wolkenhauer, O. (2006). Dynamics of biological systems: role of systems biology in medical research. *Expert Rev. Mol. Diagn.* *6*, 891–902.
- Avermann, M., Tomm, C., Mateo, C., Gerstner, W., and Petersen, C.C. (2012). Microcircuits of excitatory and inhibitory neurons in layer 2/3 of mouse barrel cortex. *J. Neurophysiol.* *107*, 3116–3134.
- Bartos, M., Vida, I., and Jonas, P. (2007). Synaptic mechanisms of synchronized gamma oscillations in inhibitory interneuron networks. *Nat. Rev. Neurosci.* *8*, 45–56.
- Basar-Eroglu, C., Schmiedt-Fehr, C., Marbach, S., Brand, A., and Mathes, B. (2008). Altered oscillatory alpha and theta networks in schizophrenia. *Brain Res.* *1235*, 143–152.
- Bastos, A.M., Vezoli, J., Bosman, C.A., Schoffelen, J.-M., Oostenveld, R., Dowdall, J.R., De Weerd, P., Kennedy, H., and Fries, P. (2015). Visual areas exert feedforward and feedback influences through distinct frequency channels. *Neuron* *85*, 390–401.
- Börgers, C., and Kopell, N. (2003). Synchronization in networks of excitatory and inhibitory neurons with sparse, random connectivity. *Neural Comput.* *15*, 509–538.
- Brette, R., and Gerstner, W. (2005). Adaptive exponential integrate-and-fire model as an effective description of neuronal activity. *J. Neurophysiol.* *94*, 3637–3642.
- Brunel, N., and Wang, X.-J. (2003). What determines the frequency of fast network oscillations with irregular neural discharges? I. Synaptic dynamics and excitation-inhibition balance. *J. Neurophysiol.* *90*, 415–430.
- Bruns, A., and Eckhorn, R. (2004). Task-related coupling from high- to low-frequency signals among visual cortical areas in human subdural recordings. *Int. J. Psychophysiol.* *51*, 97–116.
- Buzsáki, G., and Wang, X.-J. (2012). Mechanisms of gamma oscillations. *Annu. Rev. Neurosci.* *35*, 203–225.
- Canolty, R.T., and Knight, R.T. (2010). The functional role of cross-frequency coupling. *Trends Cogn. Sci.* *14*, 506–515.
- Chen, G., Zhang, Y., Li, X., Zhao, X., Ye, Q., Lin, Y., Tao, H.W., Rasch, M.J., and Zhang, X. (2017). Distinct inhibitory circuits orchestrate cortical beta and gamma band oscillations. *Neuron* *96*, 1403–1418.e6.
- Cruikshank, S.J., Lewis, T.J., and Connors, B.W. (2007). Synaptic basis for intense thalamocortical activation of feedforward inhibitory cells in neocortex. *Nat. Neurosci.* *10*, 462–468.
- Deleuze, C., Paziienti, A., and Bacci, A. (2014). Autaptic self-inhibition of cortical GABAergic neurons: synaptic narcissism or useful introspection? *Curr. Opin. Neurobiol.* *26*, 64–71.
- Diamond, M.E., von Heimendahl, M., Knutsen, P.M., Kleinfeld, D., and Ahissar, E. (2008). ‘Where’ and ‘what’ in the whisker sensorimotor system. *Nat. Rev. Neurosci.* *9*, 601–612.
- El-Boustani, S., and Sur, M. (2014). Response-dependent dynamics of cell-specific inhibition in cortical networks in vivo. *Nat. Commun.* *5*, 5689.
- Engel, A.K., Fries, P., and Singer, W. (2001). Dynamic predictions: oscillations and synchrony in top-down processing. *Nat. Rev. Neurosci.* *2*, 704–716.
- Eshaghi, M., Lee, J.H., Zhu, L., Poon, S.Y., Li, J., Cho, K.-H., Chu, Z., Karuturi, R.K.M., and Liu, J. (2010). Genomic binding profiling of the fission yeast stress-activated MAPK Sty1 and the bZIP transcriptional activator Atf1 in response to H₂O₂. *PLoS ONE* *5*, e11620.
- Fanselow, E.E., Richardson, K.A., and Connors, B.W. (2008). Selective, state-dependent activation of somatostatin-expressing inhibitory interneurons in mouse neocortex. *J. Neurophysiol.* *100*, 2640–2652.
- Fries, P. (2015). Rhythms for cognition: communication through coherence. *Neuron* *88*, 220–235.
- Gentet, L.J., Avermann, M., Matyas, F., Staiger, J.F., and Petersen, C.C. (2010). Membrane potential dynamics of GABAergic neurons in the barrel cortex of behaving mice. *Neuron* *65*, 422–435.
- Gouzé, J.-L. (1998). Positive and negative circuits in dynamical systems. *J. Biol. Syst.* *6*, 11–15.
- Harris, S.L., and Levine, A.J. (2005). The p53 pathway: positive and negative feedback loops. *Oncogene* *24*, 2899–2908.
- Harris, K.D., and Mrsic-Flogel, T.D. (2013). Cortical connectivity and sensory coding. *Nature* *503*, 51–58.
- Hoffmann, J.H., Meyer, H.-S., Schmitt, A.C., Straehle, J., Weitbrecht, T., Sakmann, B., and Helmstaedter, M. (2015). Synaptic conductance estimates of the connection between local inhibitor interneurons and pyramidal neurons in layer 2/3 of a cortical column. *Cereb. Cortex* *25*, 4415–4429.
- Hong, L.E., Summerfelt, A., McMahon, R.P., Thaker, G.K., and Buchanan, R.W. (2004). Gamma/beta oscillation and sensory gating deficit in schizophrenia. *Neuroreport* *15*, 155–159.
- Hyafil, A., Giraud, A.-L., Fontolan, L., and Gutkin, B. (2015). Neural cross-frequency coupling: connecting architectures, mechanisms, and functions. *Trends Neurosci.* *38*, 725–740.
- Jadi, M.P., and Sejnowski, T.J. (2014). Cortical oscillations arise from contextual interactions that regulate sparse coding. *Proc. Natl. Acad. Sci. USA* *111*, 6780–6785.
- Javitt, D.C. (2009). Sensory processing in schizophrenia: neither simple nor intact. *Schizophr. Bull.* *35*, 1059–1064.
- Jones, E.G., and Wise, S.P. (1977). Size, laminar and columnar distribution of efferent cells in the sensory-motor cortex of monkeys. *J. Comp. Neurol.* *175*, 391–438.
- Karnani, M.M., Jackson, J., Ayzenshtat, I., Tucciarone, J., Manoocheri, K., Snider, W.G., and Yuste, R. (2016). Cooperative subnetworks of molecularly similar interneurons in mouse neocortex. *Neuron* *90*, 86–100.
- Kilavik, B.E., Ponce-Alvarez, A., Trachel, R., Confais, J., Takerkart, S., and Riehle, A. (2012). Context-related frequency modulations of macaque motor cortical LFP beta oscillations. *Cereb. Cortex* *22*, 2148–2159.
- Kim, J.-R., and Cho, K.-H. (2006). The multi-step phosphorelay mechanism of unorthodox two-component systems in *E. coli* realizes ultrasensitivity to stimuli while maintaining robustness to noises. *Comput. Biol. Chem.* *30*, 438–444.

- Kim, D., Kwon, Y.K., and Cho, K.H. (2007). Coupled positive and negative feedback circuits form an essential building block of cellular signaling pathways. *BioEssays* 29, 85–90.
- Kim, J.-R., Shin, D., Jung, S.H., Heslop-Harrison, P., and Cho, K.-H. (2010). A design principle underlying the synchronization of oscillations in cellular systems. *J. Cell Sci.* 123, 537–543.
- Ko, H., Cossell, L., Baragli, C., Antolik, J., Clopath, C., Hofer, S.B., and Mrsic-Flogel, T.D. (2013). The emergence of functional microcircuits in visual cortex. *Nature* 496, 96–100.
- Koh, Y., Shin, K.S., Kim, J.S., Choi, J.-S., Kang, D.-H., Jang, J.H., Cho, K.-H., O'Donnell, B.F., Chung, C.K., and Kwon, J.S. (2011). An MEG study of alpha modulation in patients with schizophrenia and in subjects at high risk of developing psychosis. *Schizophr. Res.* 126, 36–42.
- Lee, K., Loros, J.J., and Dunlap, J.C. (2000). Interconnected feedback loops in the *Neurospora* circadian system. *Science* 289, 107–110.
- Lee, S., Kruglikov, I., Huang, Z.J., Fishell, G., and Rudy, B. (2013). A disinhibitory circuit mediates motor integration in the somatosensory cortex. *Nat. Neurosci.* 16, 1662–1670.
- Lefort, S., Tamm, C., Floyd Sarria, J.C., and Petersen, C.C. (2009). The excitatory neuronal network of the C2 barrel column in mouse primary somatosensory cortex. *Neuron* 61, 301–316.
- Marco, E.J., Hinkley, L.B., Hill, S.S., and Nagarajan, S.S. (2011). Sensory processing in autism: a review of neurophysiologic findings. *Pediatr. Res.* 69, 48R–54R.
- Michalareas, G., Vezoli, J., van Pelt, S., Schoffelen, J.-M., Kennedy, H., and Fries, P. (2016). Alpha-beta and gamma rhythms subserve feedback and feed-forward influences among human visual cortical areas. *Neuron* 89, 384–397.
- Milo, R., Shen-Orr, S., Itzkovitz, S., Kashtan, N., Chklovskii, D., and Alon, U. (2002). Network motifs: simple building blocks of complex networks. *Science* 298, 824–827.
- Murray, P.J., Kang, J.-W., Mirams, G.R., Shin, S.-Y., Byrne, H.M., Maini, P.K., and Cho, K.-H. (2010). Modelling spatially regulated β -catenin dynamics and invasion in intestinal crypts. *Biophys. J.* 99, 716–725.
- Neske, G.T., Patrick, S.L., and Connors, B.W. (2015). Contributions of diverse excitatory and inhibitory neurons to recurrent network activity in cerebral cortex. *J. Neurosci.* 35, 1089–1105.
- Park, S.G., Lee, T., Kang, H.Y., Park, K., Cho, K.-H., and Jung, G. (2006). The influence of the signal dynamics of activated form of IKK on NF- κ B and anti-apoptotic gene expressions: a systems biology approach. *FEBS Lett.* 580, 822–830.
- Pfeffer, C.K., Xue, M., He, M., Huang, Z.J., and Scanziani, M. (2013). Inhibition of inhibition in visual cortex: the logic of connections between molecularly distinct interneurons. *Nat. Neurosci.* 16, 1068–1076.
- Pi, H.-J., Hangya, B., Kvitsiani, D., Sanders, J.I., Huang, Z.J., and Kepecs, A. (2013). Cortical interneurons that specialize in disinhibitory control. *Nature* 503, 521–524.
- Pomerening, J.R., Kim, S.Y., and Ferrell, J.E., Jr. (2005). Systems-level dissection of the cell-cycle oscillator: bypassing positive feedback produces damped oscillations. *Cell* 122, 565–578.
- Prill, R.J., Iglesias, P.A., and Levchenko, A. (2005). Dynamic properties of network motifs contribute to biological network organization. *PLoS Biol.* 3, e343.
- Rickert, J., Oliveira, S.C., Vaadia, E., Aertsen, A., Rotter, S., and Mehring, C. (2005). Encoding of movement direction in different frequency ranges of motor cortical local field potentials. *J. Neurosci.* 25, 8815–8824.
- Schroeder, C.E., and Lakatos, P. (2009). Low-frequency neuronal oscillations as instruments of sensory selection. *Trends Neurosci.* 32, 9–18.
- Schröter, M., Paulsen, O., and Bullmore, E.T. (2017). Micro-connectomics: probing the organization of neuronal networks at the cellular scale. *Nat. Rev. Neurosci.* 18, 131–146.
- Shin, D., and Cho, K.-H. (2013). Recurrent connections form a phase-locking neuronal tuner for frequency-dependent selective communication. *Sci. Rep.* 3, 2519.
- Shin, S.-Y., Choo, S.-M., Kim, D., Baek, S.J., Wolkenhauer, O., and Cho, K.-H. (2006). Switching feedback mechanisms realize the dual role of MCIP in the regulation of calcineurin activity. *FEBS Lett.* 580, 5965–5973.
- Sreenath, S.N., Cho, K.-H., and Wellstead, P. (2008). Modelling the dynamics of signalling pathways. *Essays Biochem.* 45, 1–28.
- Tian, X.-J., Zhang, X.-P., Liu, F., and Wang, W. (2009). Interlinking positive and negative feedback loops creates a tunable motif in gene regulatory networks. *Phys. Rev. E Stat. Nonlin. Soft Matter Phys.* 80, 011926.
- Tsai, T.Y.-C., Choi, Y.S., Ma, W., Pomerening, J.R., Tang, C., and Ferrell, J.E., Jr. (2008). Robust, tunable biological oscillations from interlinked positive and negative feedback loops. *Science* 321, 126–129.
- Urban-Ciecko, J., and Barth, A.L. (2016). Somatostatin-expressing neurons in cortical networks. *Nat. Rev. Neurosci.* 17, 401–409.
- van Atteveldt, N., Murray, M.M., Thut, G., and Schroeder, C.E. (2014). Multi-sensory integration: flexible use of general operations. *Neuron* 81, 1240–1253.
- Voytek, B., Canolty, R.T., Shestyuk, A., Crone, N.E., Parvizi, J., and Knight, R.T. (2010). Shifts in gamma phase-amplitude coupling frequency from theta to alpha over posterior cortex during visual tasks. *Front. Hum. Neurosci.* 4, 191.
- Wilson, H.R., and Cowan, J.D. (1972). Excitatory and inhibitory interactions in localized populations of model neurons. *Biophys. J.* 12, 1–24.
- Womelsdorf, T., and Everling, S. (2015). Long-range attention networks: circuit motifs underlying endogenously controlled stimulus selection. *Trends Neurosci.* 38, 682–700.
- Womelsdorf, T., Valiante, T.A., Sahin, N.T., Miller, K.J., and Tiesinga, P. (2014). Dynamic circuit motifs underlying rhythmic gain control, gating and integration. *Nat. Neurosci.* 17, 1031–1039.
- Yang, W., Carrasquillo, Y., Hooks, B.M., Nerbonne, J.M., and Burkhalter, A. (2013). Distinct balance of excitation and inhibition in an interareal feedforward and feedback circuit of mouse visual cortex. *J. Neurosci.* 33, 17373–17384.
- Zhang, S., Xu, M., Kamigaki, T., Hoang Do, J.P., Chang, W.-C., Jenvay, S., Miyamichi, K., Luo, L., and Dan, Y. (2014). Selective attention. Long-range and local circuits for top-down modulation of visual cortex processing. *Science* 345, 660–665.

STAR★METHODS

KEY RESOURCES TABLE

REAGENT or RESOURCE	SOURCE	IDENTIFIER
Deposited Data		
MATLAB code and data used in this study	This paper	http://sbie.kaist.ac.kr/software
Software and Algorithms		
MATLAB R2014a	MathWorks	https://www.mathworks.com/ ; RRID: SCR_001622

CONTACT FOR REAGENT AND RESOURCE SHARING

Further information and requests for resources should be directed to and will be fulfilled by the Lead Contact, Kwang-Hyun Cho (ckh@kaist.ac.kr)

METHOD DETAILS

Network model

The network model was constructed with four neuronal classes (PCs, PV INs, SST INs, and VIP INs). A total of 1600 neurons were used to describe the network, divided into 1200 PCs, 160 PV INs, 120 SST INs, and 120 VIP INs. The number of neurons in each class were chosen by following experimentally determined values (Gentet et al., 2010; Lefort et al., 2009). All neurons were described by the conductance-based adaptive exponential integrate and fire model (AdEx) (Brette and Gerstner, 2005). The membrane potential $V_{m,i}$ of neuron i was described with the following equation

$$C \frac{dV_{m,i}}{dT} = -g_l(V_{m,i} - E_l) + g_l \Delta \tau e^{\left(\frac{V_{m,i} - V_T}{\Delta \tau}\right)} - w_{ad} - g_{PC}(V_{m,i} - E_{syn,e}) - g_{PV}(V_{m,i} - E_{syn,i}) - g_{SST}(V_{m,i} - E_{syn,i}) - g_{VIP}(V_{m,i} - E_{syn,i}), \quad i \in [1 - 1600]$$

where $V_{m,i}, i \in [1 - 1200]$, $V_{m,i}, i \in [1 - 1360]$, $V_{m,i}, i \in [1361 - 1480]$, $V_{m,i}, i \in [1481 - 1600]$ correspond to membrane potential of PCs, PV INs, SST INs and VIP INs population, respectively. The adaptation current w_{ad} was described by

$$\tau_{w_{ad}} \frac{dw_{ad}}{dT} = a(V_{m,i} - E_l) - w_{ad}$$

where $\tau_{w_{ad}}$ is the time constant of the adaptation of a neuron and a is the adaptation parameter. When the membrane potential V_m reaches the spike threshold V_T , a spike is emitted, and V_m is reset to the resting membrane potential V_{rest} , whereas w_{ad} is incremented by an amount b . Experimentally determined values for electrophysiological properties were used to represent the class-specific neurons (see Table S1) (El-Boustani and Sur, 2014; Ko et al., 2013; Neske et al., 2015). Respect to the adaptation current, a and b for PC, SST, VIP class were set as 2 nS, 2 nS, -1 nS and 4 pA, 4 pA, 19 pA, respectively. $\tau_{w_{ad}}$ was set to 120 ms for PC, SST, and VIP. For PV class, the adaptation current was set to zero as the PV class shows weak adaptation (Pfeffer et al., 2013).

Synaptic interaction modeling

Experimentally recorded average unitary postsynaptic potential (uPSP) amplitudes and kinetics (Avermann et al., 2012; Neske et al., 2015) were used to estimate the synaptic properties between the pre- and postsynaptic neuronal populations. The synaptic conductance profile $g_{syn}(t)$ was modeled as a sum of two exponentials, one for rising and the other for the decaying phase with the time constant τ_{rise} and τ_{decay} . Minimization of the mean square error between the estimated uPSP and the experimentally determined uPSP served as a cost function to optimize the synaptic parameters ($g_{syn,max}, \tau_{rise}, \tau_{decay}$) (Hoffmann et al., 2015). The estimated synaptic parameters are summarized in Table S2. The conductance changes by arrival of the j^{th} spike from the presynaptic input stream S was described by

$$g_{syn}(t) = \sum_{j=1}^n \left(g_{syn,max} \times N \times \left(\exp\left(-\frac{t-t_j}{\tau_{decay}}\right) - \exp\left(-\frac{t-t_j}{\tau_{rise}}\right) \right) \right), \quad S = [t_1, t_2, \dots, t_n]$$

The normalization factor N ensures that g_{syn} is equals to $g_{syn,max}$ at $t = t_{peak}$ where t_{peak} and N were described by

$$t_{peak} = t_j + \frac{\tau_{decay}\tau_{rise}}{\tau_{decay} - \tau_{rise}} \ln\left(\frac{\tau_{decay}}{\tau_{rise}}\right),$$

$$N = \frac{1}{\exp(- (t_{peak} - t_i) / \tau_{decay}) - \exp(- (t_{peak} - t_i) / \tau_{rise})}$$

The unitary postsynaptic current (uPSC) and resultant unitary postsynaptic charge (uPSQ, the time integral of the uPSC) evoke by single presynaptic spike were described by

$$I_{syn}(t) = g_{syn}(t)(V_{m,i} - E_{syn}),$$

$$Q_{syn} = \sum_t I_{syn}(t)$$

which are summarized in [Table S2](#). The connectivity specificity of each neuronal class as a postsynaptic population was described by setting the synaptic conductance g_{syn} of unwired neuronal classes to zero as follows: $g_{VIP} = 0$ for $i \in [1 - 1200]$, $g_{VIP} = 0$ for $i \in [1201 - 1360]$, $g_{SST} = g_{PV} = 0$ for $i \in [1361 - 1480]$, and $g_{PC} = g_{VIP} = g_{PV} = 0$ for $i \in [1481 - 1600]$; thus, the unwired neuronal classes do not influence the V_m changes of that neuronal class. Exceptionally, synaptic conductance profile of g_{SST} for $i \in [1361 - 1480]$ and g_{VIP} for $i \in [1481 - 1600]$ was calculated to examine contribution of self-inhibition connection on the SST INs and VIP INs, respectively.

External inputs

To mimic the local feed-forward input from the inter-layer, 150 presynaptic Poisson neurons with firing rates of 40 spikes/s were projected onto PCs, PV INs, SST INs and VIP INs with $Pcon_{LOCAL-PC} = 0.2$, $Pcon_{LOCAL-PV} = 0.01$, $Pcon_{LOCAL-SST} = 0.01$, $Pcon_{LOCAL-VIP} = 0.01$ for all simulations. Connection probabilities were chosen to create oscillatory behaviors on NF_{PC-SST} , and NF_{PC-PV} , respectively. An additional 150 Poisson neurons with varying firing rate from 0 spikes/s to 150spikes/s with 2 spikes/s increment were projected exclusively to the VIP INs with a $Pcon_{TOP_DOWN-VIP} = 0.3$ to mimic the top-down input from a higher-order cortex.

Conditions for generating oscillations in NF_{PC-SST} and NF_{PC-PV}

Connection probability (Pcon) of the excitatory and inhibitory connections within the two nested negative feedback structures (NF_{PC-SST} and NF_{PC-PV}) were chosen to generate synchronized oscillatory activity of PCs. We divided the PCs population into two equal sub-populations, assuming that one population is involved in generating slow oscillation, and another population is involved in generating fast oscillation. These two sub-populations of PCs were connected through an excitatory connection of $Pcon_{PC \rightarrow PC} = 0.02$ to influence each other. Following criteria were used to select the Pcon for each pathway in NF_{PC-SST} and NF_{PC-PV} : i) a Pcon combination that generates oscillatory activity of PCs (characterization of oscillatory activity is described in *Characterization of oscillations* below), ii) a Pcon combination that provides high synchrony in the population activity of PCs (measured by calculating synchronoization index ([Shin and Cho, 2013](#))). Using numerical simulations, we chose the specific Pcon combination of $Pcon_{SST \rightarrow PC} = 0.36$, $Pcon_{PC \rightarrow SST} = 0.18$ and $Pcon_{PV \rightarrow PC} = 0.53$, $Pcon_{PC \rightarrow PV} = 0.4$, $Pcon_{PV \rightarrow PV} = 0.75$ that generates highly synchronized and experimentally observed slow (18 Hz) and fast (75 Hz) oscillations, respectively ([Chen et al., 2017](#)) (see [Figure S2](#)).

Characterization of oscillations

The population activity of PCs was characterized as either rhythmic-mode (i.e., oscillatory mode) or asynchronous-mode (i.e., non-oscillatory mode) according to the following rhythmicity criteria: The spike-time histogram (its definition is described in the *Data analysis* section below) of PCs was low-pass filtered with a cutoff frequency of 100 Hz using fifth-order Butterworth filters in the MATLAB signal-processing-toolbox. The amplitude of each frequency component of the histogram was detected by Fast Fourier Transform (FFT) using the `fft` command in MATLAB 2014a. A dominant (or characteristic) frequency component was considered present if the power spectrum includes a peak amplitude that is at least 30% larger than the amplitudes of any other frequency components. Depending on the existence of the dominant frequency component, we characterized PCs' response as either rhythmic-mode (if the dominant frequency component exists) or asynchronous-mode (if the dominant frequency does not exist). The dominant frequency component of the histogram in rhythmic-mode was estimated again using the `findpeaks` command in MATLAB 2014a, where the `findpeaks` command detects and counts the number of local peaks in the smoothed histogram to estimate the frequency.

Frequency modulation tendency

Frequency modulation tendency (FMT) is the index that measures the adaptability of the IPNF structure for top-down input, which is calculated by counting the number of different frequency components that appear in the predetermined top-down input strength range. For [Figures 2B–2D](#) and [3](#), the FMT of the IPNF structure was measured over top-down input strengths from 0 spikes/s to 120 spikes/s with 2 spikes/s increment (total 61 different stimulation strengths). For [Figure 4C](#), the range of top-down stimuli was increased from 0 spikes/s to 150 spikes/s with 2 spikes/s increments (total of 76 different strengths) to determine the FMT of the IPNF structure before the state transition from the SST-dominated state to the PV-dominated state occurs. The occurrence of the

state transition was determined by checking the oscillation frequency of PCs changing from low frequency (under 20 Hz; controlled by SST INs) to high frequency (over 50 Hz; controlled by PV INs).

Quantification of phase-amplitude coupling

The strength of phase-amplitude coupling (PAC) was quantified by using the *Envelope-to-Signal Correlation (ESC) measure* (Bruns and Eckhorn, 2004). The ESC quantifies the strength of PAC by calculating the correlation between the amplitude envelope of the band-pass filtered high frequency signal and the band-pass filtered low frequency signal.

Quantification of noise vulnerability of phase-amplitude coupling with respect to amplitude-frequency relationships of slow oscillations

The artificial phase-amplitude coupling (PAC) signals were generated by following procedures (Figure S5A): First, we extracted the instantaneous phase and computed the envelope signal of slow oscillation. Second, we multiplied the envelope of slow oscillation with the fast oscillation so that the amplitude of fast oscillation is modulated by the phase of slow oscillation. Lastly, we combined the slow oscillation and the amplitude-modulated fast oscillation to generate a PAC signal.

Three cases of *amplitude-frequency relationships* were tested to see the potential benefit of maintaining the amplitude constant during frequency modulation of slow oscillation (Figures S5 and S6). The frequencies examined were 4Hz, 6Hz, 8Hz, 10Hz, 12Hz, and 14Hz, which are in the theta-alpha frequencies that are reported to create PAC signals with gamma frequency oscillations (Hyafil et al., 2015; Voytek et al., 2010). The amplitudes of slow oscillations were modulated in a range from 0.2 to 5 times the default amplitude strength. The following describes the three *amplitude-frequency relationships* (Figure S5B):

1. Case 1 (Amplitude maintains while frequency increases): Even if the frequency is modulated, the amplitude is fixed at the default amplitude strength.
2. Case 2 (Amplitude increases when frequency increases): As the frequency increases, the amplitude also increases. As a result, a 4 Hz oscillation will have an amplitude that is 0.2 times larger (i.e., 5 times less) than the default amplitude strength, and a 14 Hz oscillation will have an amplitude five times larger than the default amplitude strength.
3. Case 3 (Amplitude decreases when frequency increases): As the frequency increases, the amplitude decreases. Thus, a 4 Hz signal will have an amplitude five times larger than the amplitude of the default amplitude strength, and a 14 Hz signal will have an amplitude of 0.2 times larger (i.e., 5 times less) than the default amplitude strength.

Changes in coupling strengths of PAC signals for each of the three cases were examined by adding noise to the slow oscillations (of different frequencies) before extracting their phase components and creating PAC signals with 60 Hz fast oscillation. The noise level is given from 0 to 0.7 times the default amplitude strength (Figure S5D; it is conceivable to assume that the noise level is proportional to the distance between distinct areas that generate low and fast oscillations).

Data analysis

Network simulations, data analysis, and visualizations were done with MATLAB 2014a (The MathWorks). For each simulation condition, neuronal population activity of 1.5 s was simulated over 50 trials to assure the reliability/reproducibility of the output response of the model. Considering the settling time, an initial 500 ms of simulation data were removed. Data analysis was performed on the remaining 1 s of simulation data by computing spike-time histogram of PCs. The spike-time histogram is an estimate for the time-varying firing rate of neuronal population. It was obtained by dividing the firing activity of PCs into discrete time bin of 2ms and counting the number of spikes that fell in each time bin. The mean firing rate was calculated by counting the number of spikes evoked during 1 s and averaged over the trials. The mean oscillation amplitude was measured by averaging the amplitudes of the spike-time histogram (which is corresponding to spikes/ms) within the 5% of the maximum amplitude.

QUANTIFICATION AND STATISTICAL ANALYSIS

In all analyses, box-and-whisker plots are presented. All the analyses were performed using MATALB 2014a. Details of data analysis are documented in [METHOD DETAILS](#).

DATA AND SOFTWARE AVAILABILITY

Codes and data used in this study can be found at <http://sbie.kaist.ac.kr/software>.

Cell Reports, Volume 25

Supplemental Information

**Combined Positive and Negative Feedback Allows
Modulation of Neuronal Oscillation Frequency
during Sensory Processing**

Byeongwook Lee, Dongkwan Shin, Steven P. Gross, and Kwang-Hyun Cho

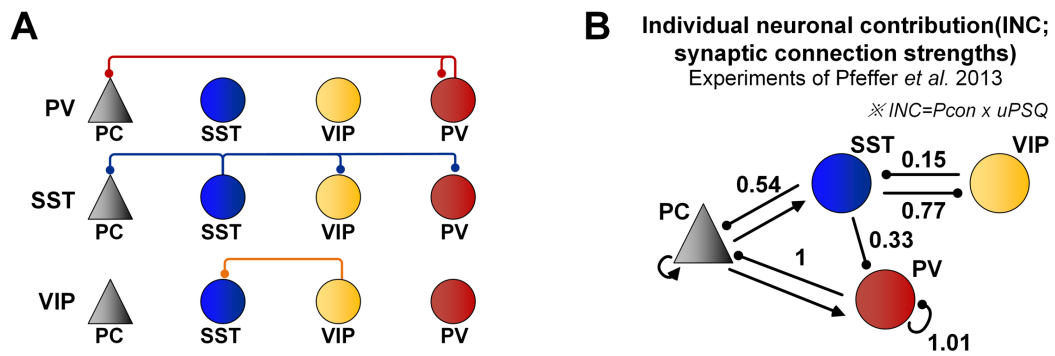


Figure S1. Connectivity properties of heterogeneous interneuron classes in the layer 2/3 of the sensory cortex. Related to Figure 1.

(A) Schematic of the connectivity patterns of the three interneuron (IN) classes (PV, SST, and VIP expressing interneurons) in the layer 2/3 of the sensory cortex. PV INs preferentially inhibit one another; SST INs inhibit all other classes of INs but avoids inhibiting themselves, and VIP INs preferentially inhibit SST INs. **(B)** Net synaptic contribution (calculated by the measure named *individual neuronal contribution*) of the presynaptic IN classes to postsynaptic neuronal classes adapted from **Figure 7A** in Pfeffer *et al.*, 2013. INC is calculated by multiplying connection probability (P_{con}) between pre- and postsynaptic neuronal populations and unitary postsynaptic charge (u_{PSQ}) generated by single presynaptic spike. INC of each pathway is normalized by $INC_{PV \rightarrow PC}$.

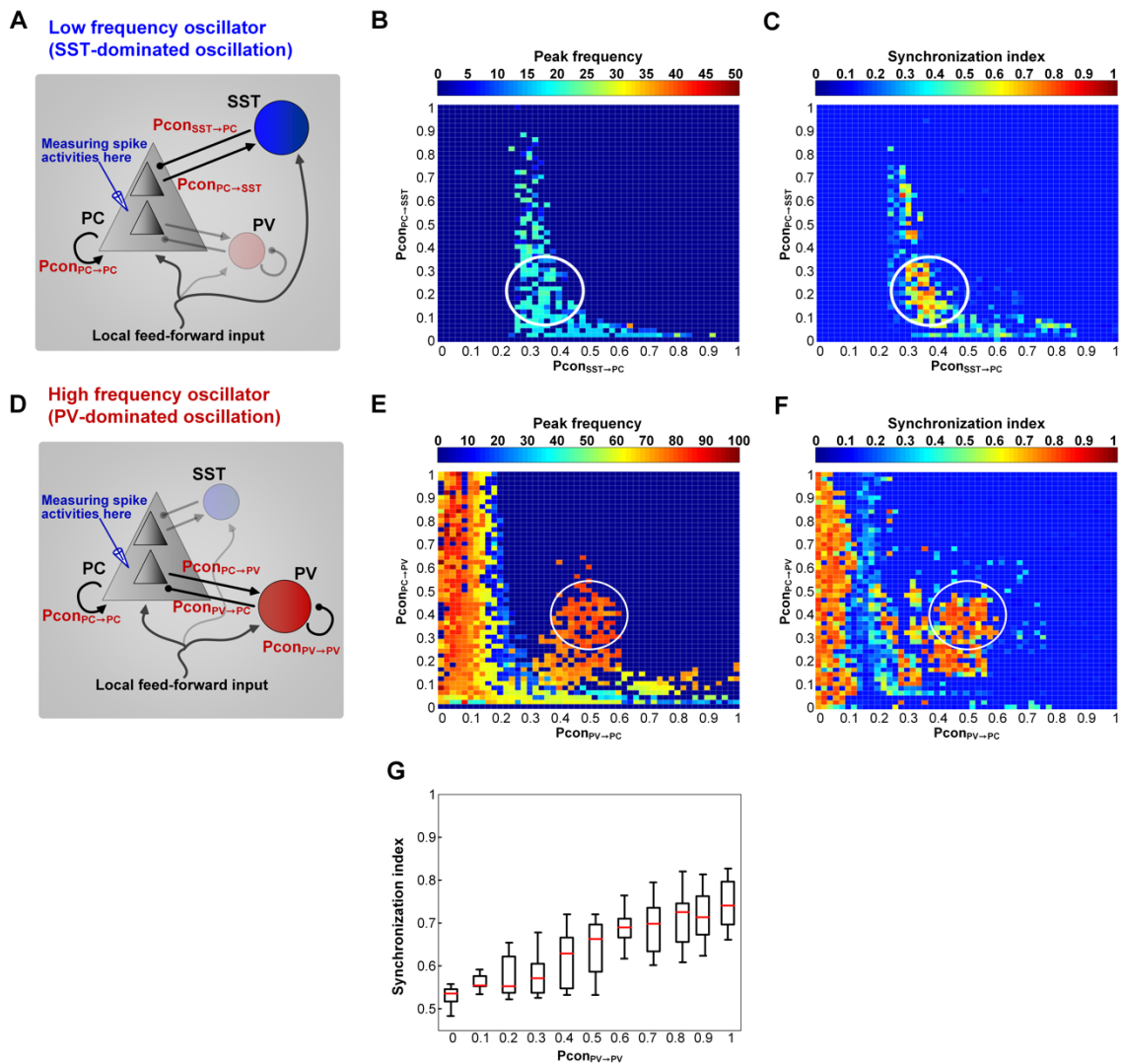


Figure S2. Conditions for generating oscillations in NF_{PC-SST} and NF_{PC-PV} . Related to Figure 1.

(A) Schematic of the NF_{PC-SST} . (B-C) Peak frequency and synchronization index of the PCs' population firing activity were measured for every Pcon combinations in the NF_{PC-SST} . We chose specific Pcon combination of $P_{con_{SST \rightarrow PC}}=0.36$ and $P_{con_{PC \rightarrow SST}}=0.18$ that generates 18 Hz oscillation with high synchrony (indicated with white circles). (D) Schematic of the NF_{PC-PV} . (E-F) Peak frequency and synchronization index of the PCs' population firing activity were measured for every Pcon combinations in the NF_{PC-PV} . We chose specific Pcon combination of $P_{con_{PV \rightarrow PC}}=0.53$, $P_{con_{PC \rightarrow PV}}=0.4$ and $P_{con_{PV \rightarrow PV}}=0.75$ that generates 75 Hz oscillation with high synchrony (indicated with white circles). (G) Changes in synchronization index related to the self-inhibitory connections within PV INs.

Checking frequency modulation tendency of the IPNF structure depending on feedback strength between SST INs and VIP INs

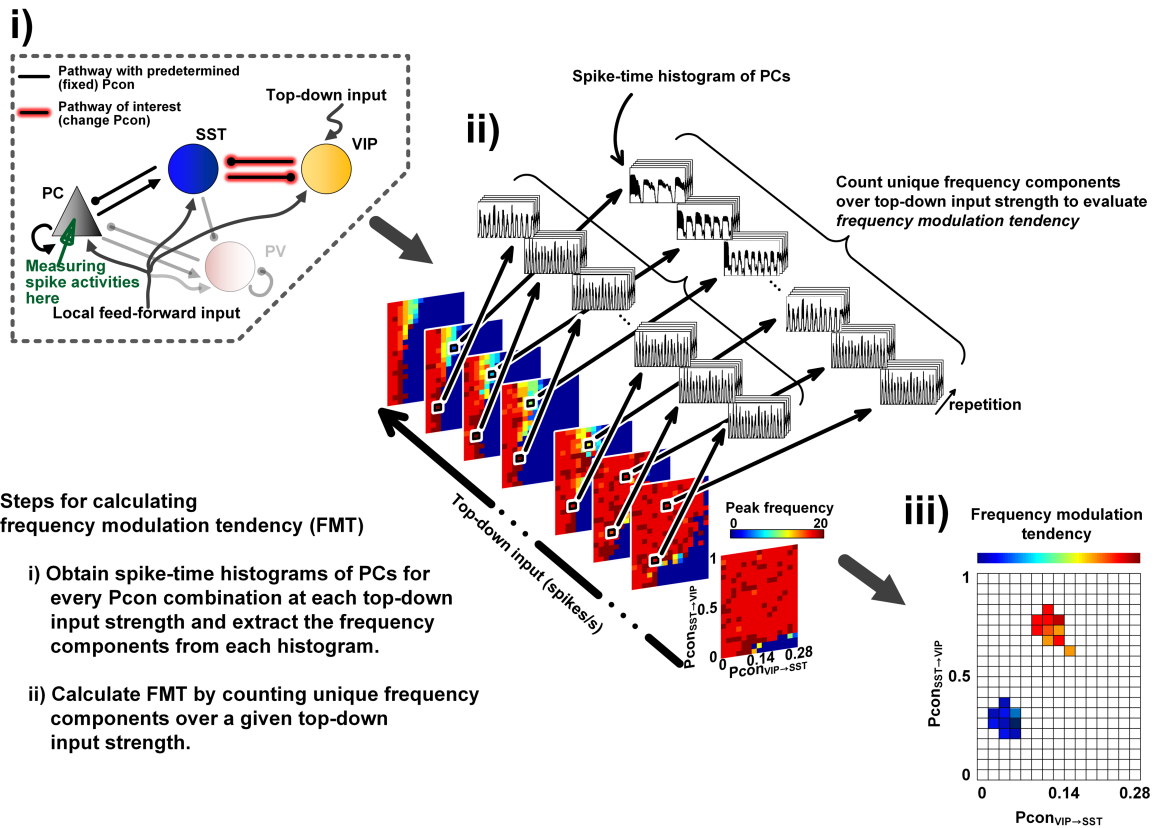


Figure S3. An example illustration of calculating frequency modulation tendency (FMT) of the IPNF structure. Related to Figure 2.

Frequency modulation tendencies (FMTs) of the IPNF structure with particular connectivity strengths (i.e., connection probability; Pcon) were calculated by counting the number of different frequency components that appear in the predetermined top-down input strength range. In this figure, we illustrated the overall steps for searching the particular connection probabilities between SST INs and VIP INs (i.e., $P_{con_{SST \rightarrow VIP}}$, $P_{con_{VIP \rightarrow SST}}$) that provide maximum FMT.

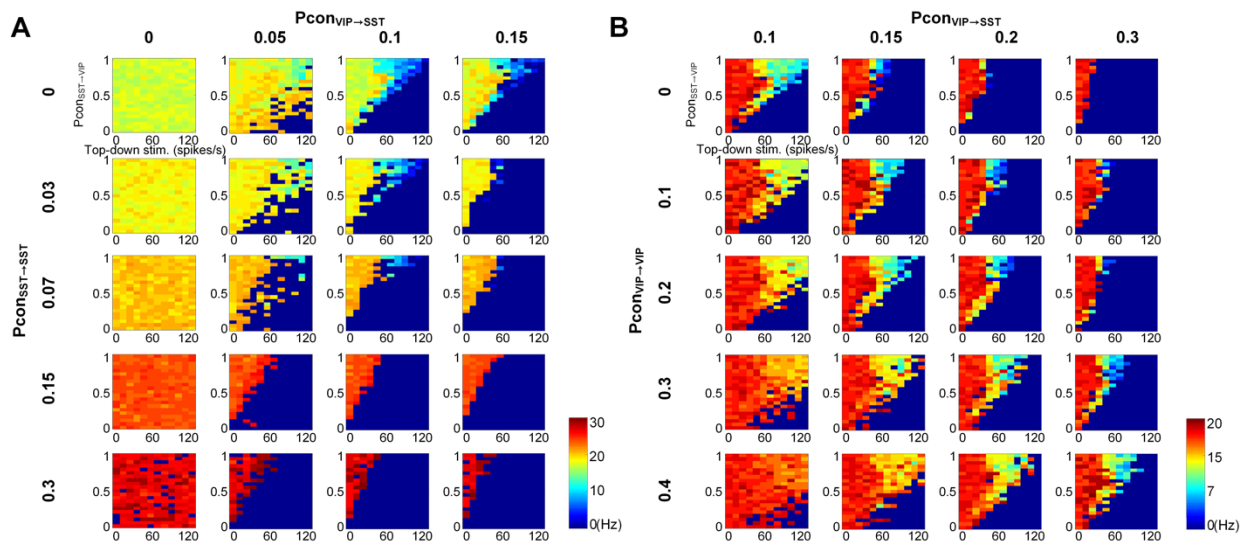


Figure S4. Variation in the frequency modulation tendency (FMT) of the IPNF structure under increasing self-inhibition on SST and VIP interneurons. Related to Figure 3.

(A) Self-inhibition connectivity of the SST interneurons is modulated by varying $P_{\text{conSST} \rightarrow \text{SST}}$. When the $\text{VIP} \rightarrow \text{SST}$ pathway is disconnected ($P_{\text{conVIP} \rightarrow \text{SST}}=0$), the model generated resonant frequency (F_R) of $\text{NF}_{\text{PC-SST}}$, which is increased ($F_{R, P_{\text{conSST} \rightarrow \text{SST}:0}}=18$ Hz, $F_{R, P_{\text{conSST} \rightarrow \text{SST}:0.07}}=22$ Hz, $F_{R, P_{\text{conSST} \rightarrow \text{SST}:0.3}}=30$ Hz) with raising $P_{\text{conSST} \rightarrow \text{SST}}$. The IPNF structure with increasing $P_{\text{conSST} \rightarrow \text{SST}}$ tends to give up the rhythmic-mode after oscillating at the characteristic peak frequency (i.e., resonant frequency) of the $\text{NF}_{\text{PC-SST}}$, rather than modulating its oscillation frequency. As a result, the frequency modulation tendency (FMT) drops dramatically as the $P_{\text{conSST} \rightarrow \text{SST}}$ increases. **(B)** When increasing $P_{\text{conVIP} \rightarrow \text{VIP}}$, the IPNF structure showed a reduced FMT again, but at a different rate compared to when increasing $P_{\text{conSST} \rightarrow \text{SST}}$. As the $P_{\text{conVIP} \rightarrow \text{VIP}}$ increases, a larger $P_{\text{conVIP} \rightarrow \text{SST}}$ is required (**Figure 3D, turquoise**) to increase the FMT. However, increasing $P_{\text{conVIP} \rightarrow \text{SST}}$ causes a reduced FMT (**Figure 3D, black**), which was shown in our previous result (**Figure 2B, right bottom**). As a result, increasing self-inhibition on VIP interneurons causes a decrement in the FMT.

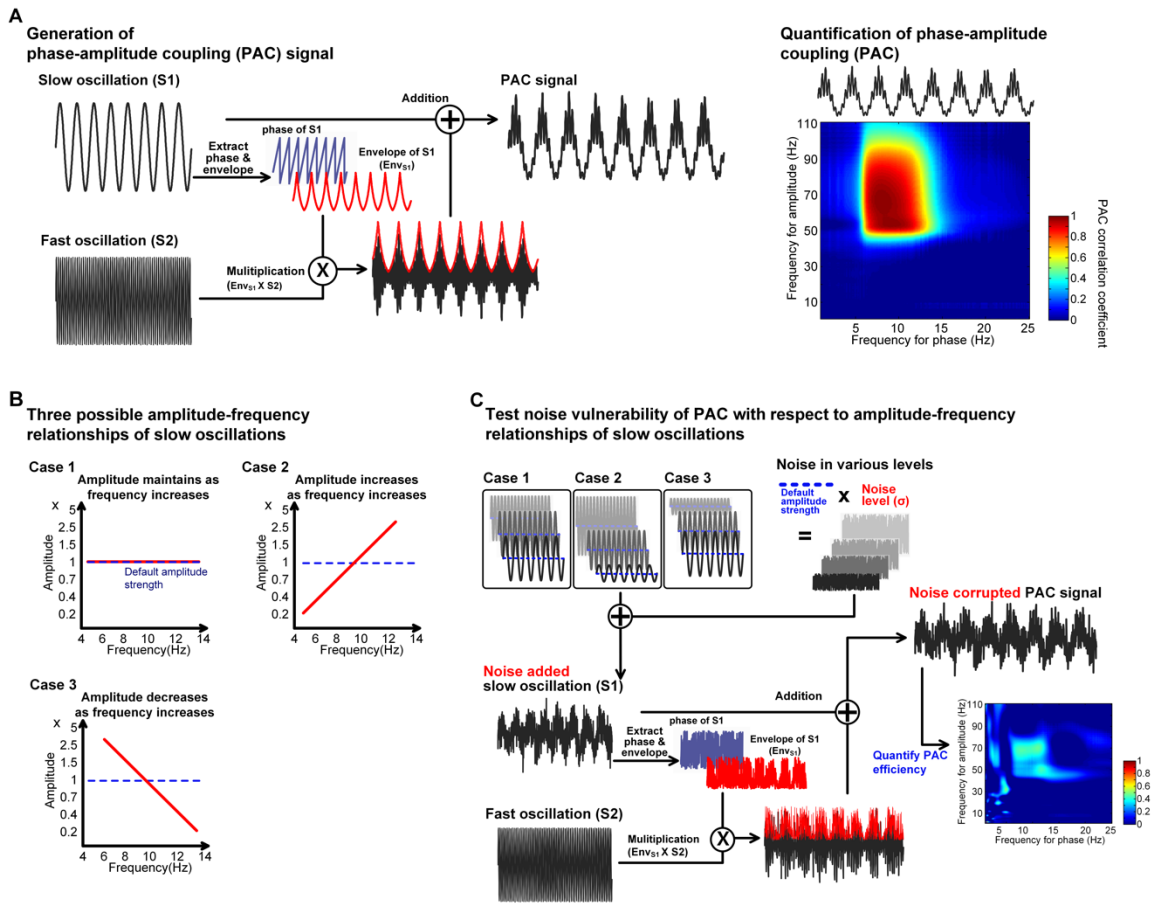


Figure S5. Experimental design to investigate the influence of various amplitude-frequency relationships of slow oscillation on phase-amplitude coupling (PAC) strength. Related to Figure 5.

(A) Generation of phase-amplitude coupling (PAC) signal (left) and quantification of PAC strength (right). **(B)** Three possible amplitude-frequency relationships of slow oscillation (see **Method Details**). **(C)** Experimental design to test noise vulnerability of PAC signal with respect to the amplitude-frequency relationships of slow oscillations.

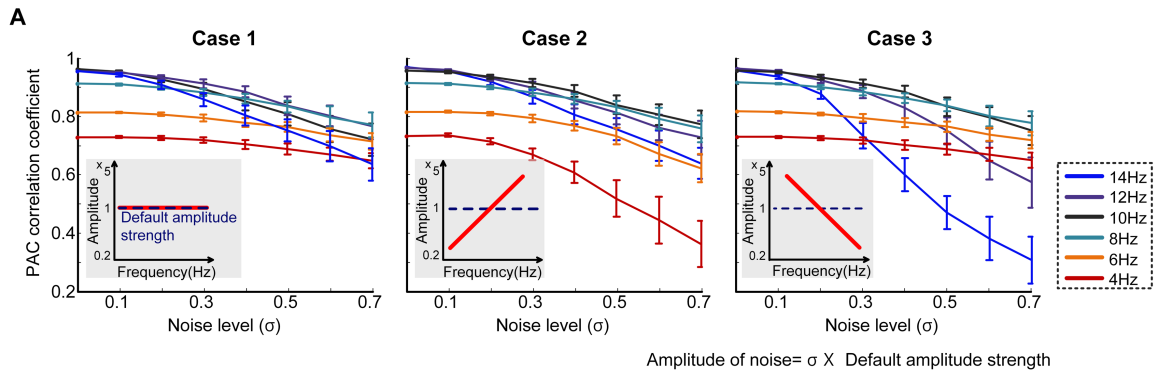


Figure S6. Quantification of noise vulnerability of phase-amplitude coupling (PAC) with respect to the amplitude-frequency relationship of slow oscillation. Related to Figure 5.

(A) Slow oscillations at six different frequencies (i.e., 4Hz, 6Hz, 8Hz, 10Hz, 12Hz, and 14Hz) were used to generate phase-amplitude coupling (PAC) signals. In Case 1, none of the generated PAC signals showed a dramatic decrease in coupling strength against noise, showing its robustness against noise. On the other hand, noticeable decreases in coupling strengths of the PAC signals created by 4 & 6 Hz and 12 & 14 Hz were observed in Case 2 (middle) and Case 3 (right), respectively. Frequency modulation of slow oscillations and the corresponding changes in PAC with gamma oscillations can be viewed as a series of processes for cognitions. It is therefore ideal to provide reliable and robust coupling PAC strengths for all slow oscillations (4H to 14 Hz). This result shows that case 1, which maintains constant amplitude over varying frequency, provides the highest reliability. Due to this aspect, maintaining the amplitude constant over varying frequency might be preferable for slow oscillations.

Table S1. Distribution of electrophysiological properties of neuronal classes in L2/3 of the sensory cortex. Related to Figure 1 & 2 & 3 & 4 & 5 & 6.

Symbol	Function	Parameter			
		PC	PV	SST	VIP
τ_m	Membrane time constant (ms)	10.5±5.1	3.1±1.3	11.8±4.6	10.9±3.8
V_T	Spike threshold (mV)	-41.5±6.0	-41.6±3.4	-41.8±6.3	-43.7±5.3
V_{reset}	Resting potential (mV)	-67.4±4.3	-66.4±3.0	-59.9±4.0	-65.7±1.9
g_l	Leak conductance (nS)	20.3±6.0	77.1±25.6	21.4±8.7	26.6±10.9
E_l	Leak reversal potential (mV)	-70			
$E_{syn,e}$	Excitatory reversal potential (mV)	0			
$E_{syn,i}$	Inhibitory reversal potential (mV)	-85			
C_m	Membrane capacitance (pF)	200			
Δ_T	Slope factor (mV)	2			

Table S2. Estimated distribution of synaptic interactions between neuronal classes in L2/3 of the sensory cortex. Related to Figure 1 & 2 & 3 & 4 & 5 & 6.

Symbol	Function	Parameters			
		Presynaptic→Postsynaptic			
uPSP	Unitary postsynaptic potential amplitude (mV)	0.37±0.1 (PC→PC)	-0.52±0.1 (PV→PC)	-0.39±0.1 (SST→PC)	-0.39±0.2 (VIP→SST)
		0.82±0.1 (PC→PV)	-0.76±0.2 (PV→PV)	-0.37±0.1 (SST→PV)	-0.49±0.2 (VIP→VIP)
		0.39±0.11 (PC→SST)		-0.49±0.2 (SST→SST)	
		0.39±0.11 (PC→VIP)		-0.39±0.1 (SST→VIP)	
$\tau_{PSP,rise}$	Rise time of uPSP kinetics (ms)	3.5±0.6 (PC→PC)	3.4±0.5 (PV→PC)	5.4±0.5 (SST→PC)	4.9±1.2 (VIP→SST)
		1.6±0.2 (PC→PV)	1.8±0.2 (PV→PV)	3.1±0.6 (SST→PV)	4.9±1.2 (VIP→VIP)
		2.6±0.5 (PC→SST)		4.9±1.2 (SST→SST)	
		2.6±0.5 (PC→VIP)		4.9±1.2 (SST→VIP)	
$\tau_{PSP,decay}$	Decay time of uPSP kinetics (ms)	28.6±4.7 (PC→PC)	40.0±4.4 (PV→PC)	52.5±7.3 (SST→PC)	32.4±12 (VIP→SST)
		11.7±1.6 (PC→PV)	16.4±4.1 (PV→PV)	16.8±4.1 (SST→PV)	32.4±12 (VIP→VIP)
		16.7±2.2 (PC→SST)		32.4±12 (SST→SST)	
		16.7±2.2 (PC→VIP)		32.4±12 (SST→VIP)	
$g_{syn,max}$	Synaptic conductance (nS)	0.39±0.04 (PC→PC)	2.8±0.2 (PV→PC)	1.4±0.42 (SST→PC)	1.8±0.48 (VIP→SST)
		2.1±0.09 (PC→PV)	7.8±0.5 (PV→PV)	2.7±0.21 (SST→PV)	2.3±0.48 (VIP→VIP)
		0.64±0.06 (PC→SST)		1.3±0.48 (SST→SST)	
		0.59±0.06 (PC→VIP)		1.5±0.48 (SST→VIP)	
τ_{rise}	Rise time of synaptic conductance (ms)	0.23±0.16 (PC→PC)	0.21±0.15 (PV→PC)	0.36±0.12 (SST→PC)	0.21±0.22 (VIP→SST)
		0.16±0.17 (PC→PV)	0.18±0.09 (PV→PV)	0.20±0.14 (SST→PV)	0.36±0.12 (VIP→VIP)
		0.25±0.17 (PC→SST)		0.32±0.22 (SST→SST)	
		0.24±0.11 (PC→VIP)		0.26±0.16 (SST→VIP)	
τ_{decay}	Decay time of synaptic conductance (ms)	6.7±1.8 (PC→PC)	6.4±1.8 (PV→PC)	13.1±2.1 (SST→PC)	13.1±1.1 (VIP→SST)
		3.3±1.6 (PC→PV)	4.6±1.7 (PV→PV)	5.2±1.8 (SST→PV)	11.3±1.8 (VIP→VIP)

		5.4±1.2 (PC→SST)		12.3±1.5 (SST→SST)	
		5.6±1.1 (PC→VIP)		10.2±0.96 (SST→VIP)	
uPSC	Unitary postsynaptic current (pA)	-14.2±2.5 (PC→PC)	19.0±2.7 (PV→PC)	93.9±1.6 (SST→PC)	8.45±1.8 (VIP→SST)
		-69.2±6.1 (PC→PV)	54.8±6.6 (PV→PV)	17.2±2.9 (SST→PV)	13.7±4.1 (VIP→VIP)
		-20.4±3.5 (PC→SST)		14.2±3.8 (SST→SST)	
		-21.2±3.4 (PC→VIP)		11.0±2.1 (SST→VIP)	
uPSQ	Absolute unitary postsynaptic charge (nC)	1.46±0.2 (PC→PC)	2.10±0.2 (PV→PC)	1.91±0.3 (SST→PC)	0.63±0.1 (VIP→SST)
		1.38±0.1 (PC→PV)	1.42±0.5 (PV→PV)	0.69±0.1 (SST→PV)	1.5±0.4 (VIP→VIP)
		1.03±0.1 (PC→SST)		1.10±0.3 (SST→SST)	
		0.99±0.1 (PC→VIP)		1.22±0.3 (SST→VIP)	